A UNITED STATES DEPARTMENT OF COMMERCE PUBLICATION

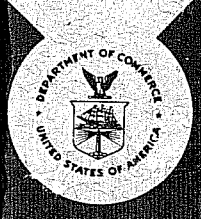

NOAA Technical Memorandum ERL ARL-32

U.S. DEPARTMENT OF COMMERCE
NATIONAL OCEANIC AND ATMOSPHERIC ADMINISTRATION
Environmental Research Laboratories

Atmospheric Transport and Diffusion in the Planetary Boundary Layer July 1970 - June 1971

Air Resources Laboratories
SILVER SPRING, MARYLAND
September 1971

ENVIRONMENTAL RESEARCH LABORATORIES

AIR RESOURCES LABORATORIES

IMPORTANT NOTICE

Technical Memoranda are used to insure prompt dissemination of special studies which, though of interest to the scientific community, may not be ready for formal publication. Since these papers may later be published in a modified form to include more recent information or research results, abstracting, citing, or reproducing this paper in the open literature is not encouraged. Contact the author for additional information on the subject matter discussed in this Memorandum.

NATIONAL OCEANIC AND ATMOSPHERIC ADMINISTRATION

U.S. DEPARTMENT OF COMMERCE
National Oceanic and Atmospheric Administration
Environmental Research Laboratories

NOAA Technical Memorandum ERL ARL-32

ATMOSPHERIC TRANSPORT AND DIFFUSION IN THE PLANETARY BOUNDARY LAYER JULY 1970 - JUNE 1971

I. Van der Hoven, Editor

Contributors

J. K. Angell
A. B. Bernstein
D. J. Bjorem
C. R. Dickson
G. A. Herbert
D. H. Pack
G. E. Start
L. L. Wendell

Annual Research Program Review
July 1970 - June 1971
for
U. S. Atomic Energy Commission

Air Resources Laboratories
Silver Spring, Maryland
September 1971

DISCLAIMER

The Environmental Research Laboratories, National Oceanic and Atmospheric Administration, U.S. Dept. of Commerce, does not approve, recommend or endorse any proprietary product or proprietary material mentioned in this publication. No reference shall be made to the Environmental Research Laboratories, or to this publication furnished by the Environmental Research Laboratories, in any advertising or sales promotion which would indicate or imply that the Environmental Research Laboratories approves, recommends or endorses any proprietary product or proprietary material mentioned herein, or which has as its purpose an intent to cause directly or indirectly the advertised product to be used or purchased because of this Environmental Research Laboratories publication.

The findings of this report are not to be construed as an official Department of Commerce position, unless so designated by other authorized documents.

PREFACE

In accordance with the letter of agreement of July 20, 1970, with the U.S. Atomic Energy Commission, Division of Reactor Development and Technology, the Air Resources Laboratories have continued their study of atmospheric transport and diffusion in the planetary boundary layer, micrometeorology, diffusion climatology, and the application of this work to the disposal of radioactive waste gases into the atmosphere. The research is technically administered and supervised through the Air Resources Environmental Laboratory of the Air Resources Laboratories. The work is performed at the Air Resources Laboratories Headquarters in Silver Spring, Maryland, and at the Air Resources Idaho Falls Laboratory, National Reactor Testing Station, Idaho. Any inquiry on the research being performed should be directed to the editor, Isaac Van der Hoven, Chief, Air Resources Environmental Laboratory, Air Resources Laboratories, National Oceanic and Atmospheric Administration, 8060 - 13th Street, Silver Spring, Maryland 20910.

CONTENTS

LIST OF FIGURES

Figure

Figure

Figure

ATMOSPHERIC TRANSPORT AND DIFFUSION IN THE PLANETARY BOUNDARY LAYER

AIR RESOURCES LABORATORIES ANNUAL RESEARCH PROGRAM
REVIEW FOR THE ENVIRONMENTAL SAFETY BRANCH
DIVISION OF REACTOR DEVELOPMENT AND TECHNOLOGY
U. S. ATOMIC ENERGY COMMISSION

JULY 1970 - JUNE 1971

1. RESEARCH AT AIR RESOURCES LABORATORIES HEADQUARTERS, SILVER SPRING, MD.

1.1 Three-Dimensional Trajectories in the Los Angeles Basin

This is a joint research effort of several Air Resources Laboratories with the sponsorship of both the Atomic Energy Commission (AEC) and the Environmental Protection Agency (EPA).

In a field program to estimate low-level, three-dimensional air trajectories in the Los Angeles Basin, constant-volume balloon (tetroon) flights associated with air quality measurements were carried out in September-October 1969. The transponder-equipped tetroons were tracked by a mobile M-33 radar (transported from the AEC National Reactor Testing Station, Idaho) positioned atop Mt. Thom just north of Glendale at 2500 ft MSL. Over the relatively flat basin, the average tetroon height was 200-300 m above the ground. A helicopter measuring oxidant values along the flight path frequently followed the tetroons. Preliminary results of the study were reported in ESSA Tech. Memo. ERLTM-ARL 20 (1970).

Figure 1 shows all trajectories of more than 1 hour duration during the experiment grouped into 6-hour categories according to the time of tetroon release. The hourly position after release is shown by consecutive numbering along each trajectory. In general the trajectories are as expected, with the trajectories directed east or north-eastward in the afternoon, due to the sea breeze, and directed nearly north during the morning due to the heating of the south-facing mountain

Figure 1. Tetroon trajectories of more than 1-hour duration in Los Angeles during Sept-Oct 1969, grouped according to time (PDT) of tetroon release. Numbers indicate hours since release.

slopes. At night the trajectories are chaotic, with air movement in various directions depending partly on the synoptic situation. In the evening, flights in the southern part of the basin move slowly eastward; whereas, further north they frequently move across the Santa Monica Mountains into the San Fernando Valley.

Tetroon flights from Redondo Beach embedded in the sea breeze almost invariably move east and then northeast as they encounter the sea breeze coming from the Long Beach area. The resulting sea breeze convergence zone moves east during the day, so that flights released in the early morning from Redondo Beach tend to move into downtown Los Angeles, and flights released later in the day move into the Azusa area, as shown by sequentially released flights 18 and 19 in the left-hand diagram of figure 2. The flights also tend to penetrate further south as the day progresses, as shown by flights 27 and 28. The right-hand diagram of figure 2 shows, in addition, how flights released from the Long Beach area move north or northwest and then northeast as they encounter the convergence zone.

Figure 3 presents the height traces of the tetroon flights as they are entrained in the sea-breeze convergence zone. Because of horizontal convergence, usually considerable upward motion occurs upon initial contact with this zone, and the vertical oscillations tend to be relatively large as the tetroon progresses northeast within the zone.

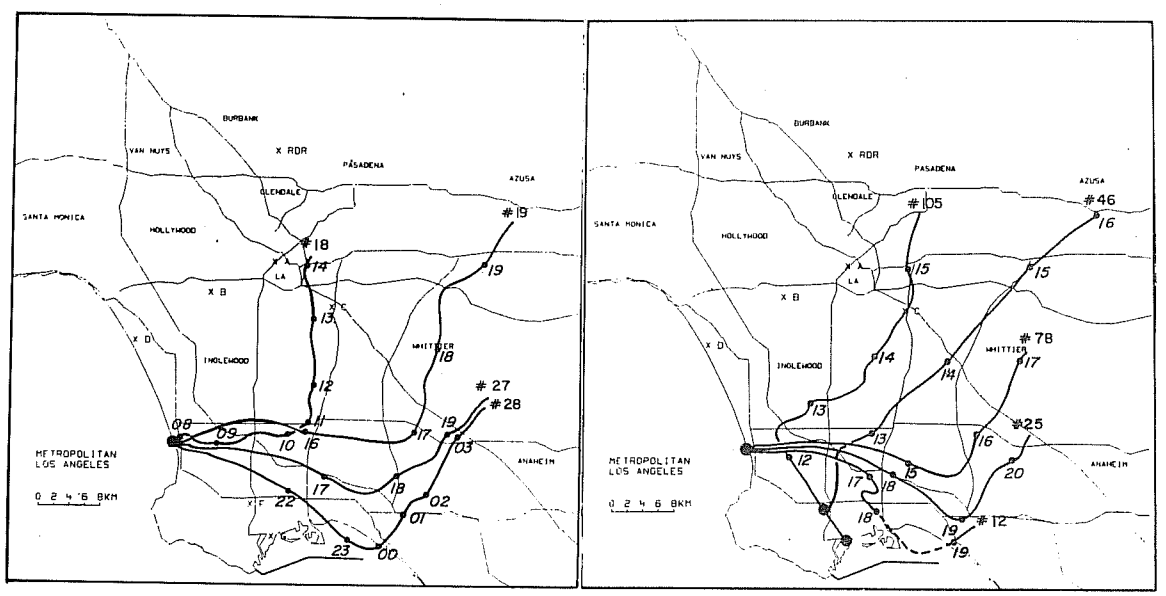

Figure 2. Daytime tetroon flights from Redondo Beach and Long Beach illustrating the convergence zone (trajectory turning) northeast of the Palos Verdes Peninsula. Numbers along trajectory are time (PDT).

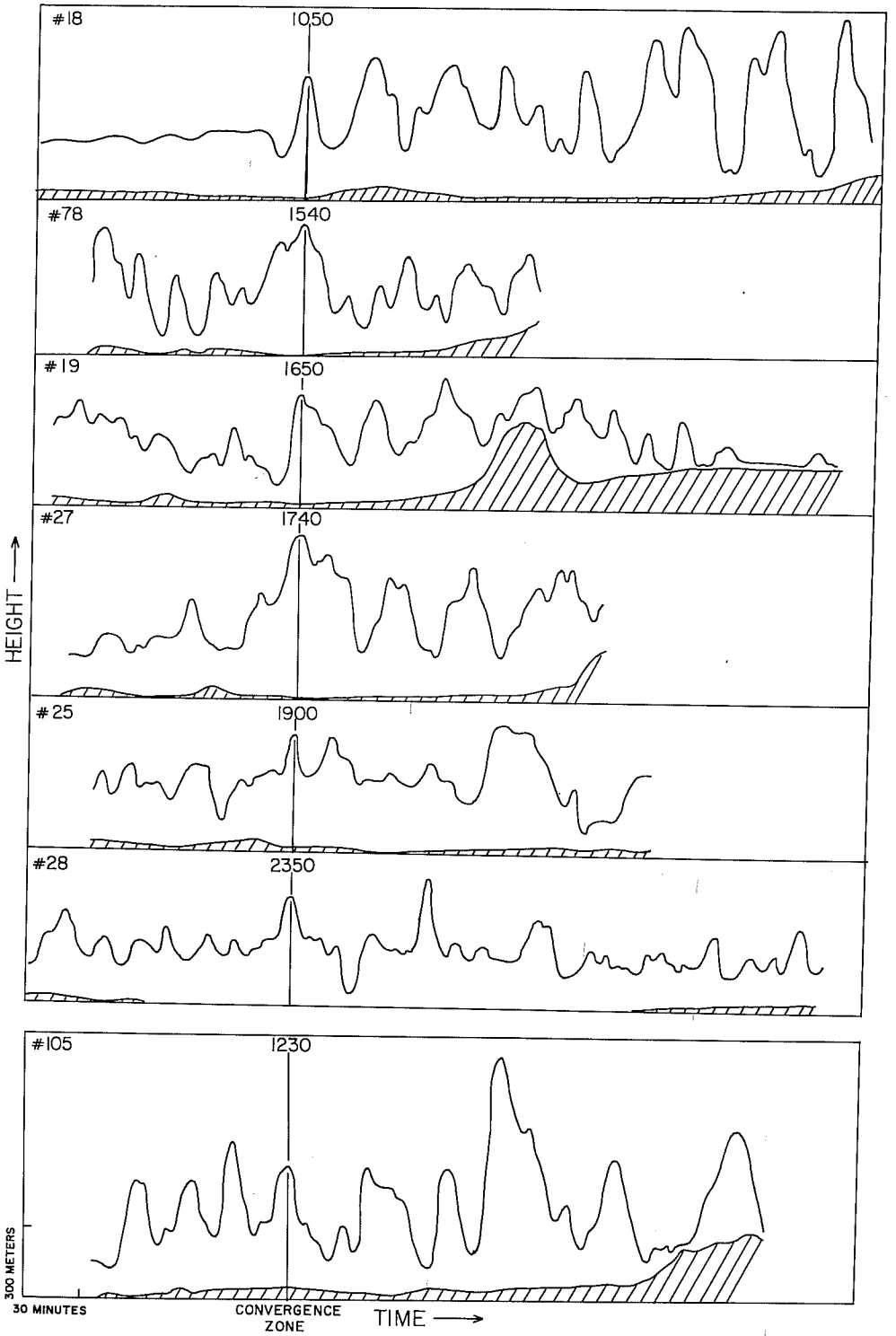

Figure 3. Tetroon height traces for flights entrained into the Palos Verdes convergence zone. Numbers along the vertical line indicate the time (PDT) of initial contact with this zone.

Two flights that exhibit stagnation and near-stagnation conditions are presented in figure 4. The numbers along the trajectories are actual position times. Flight 36 remained nearly stationary for 7 hours near Pasadena in the transition between the sea breeze regime on 2 successive days. The blow-up between 0500 PDT and 1200 PDT shows how small cyclonic and anticyclonic loops were traced out during this time. Flight

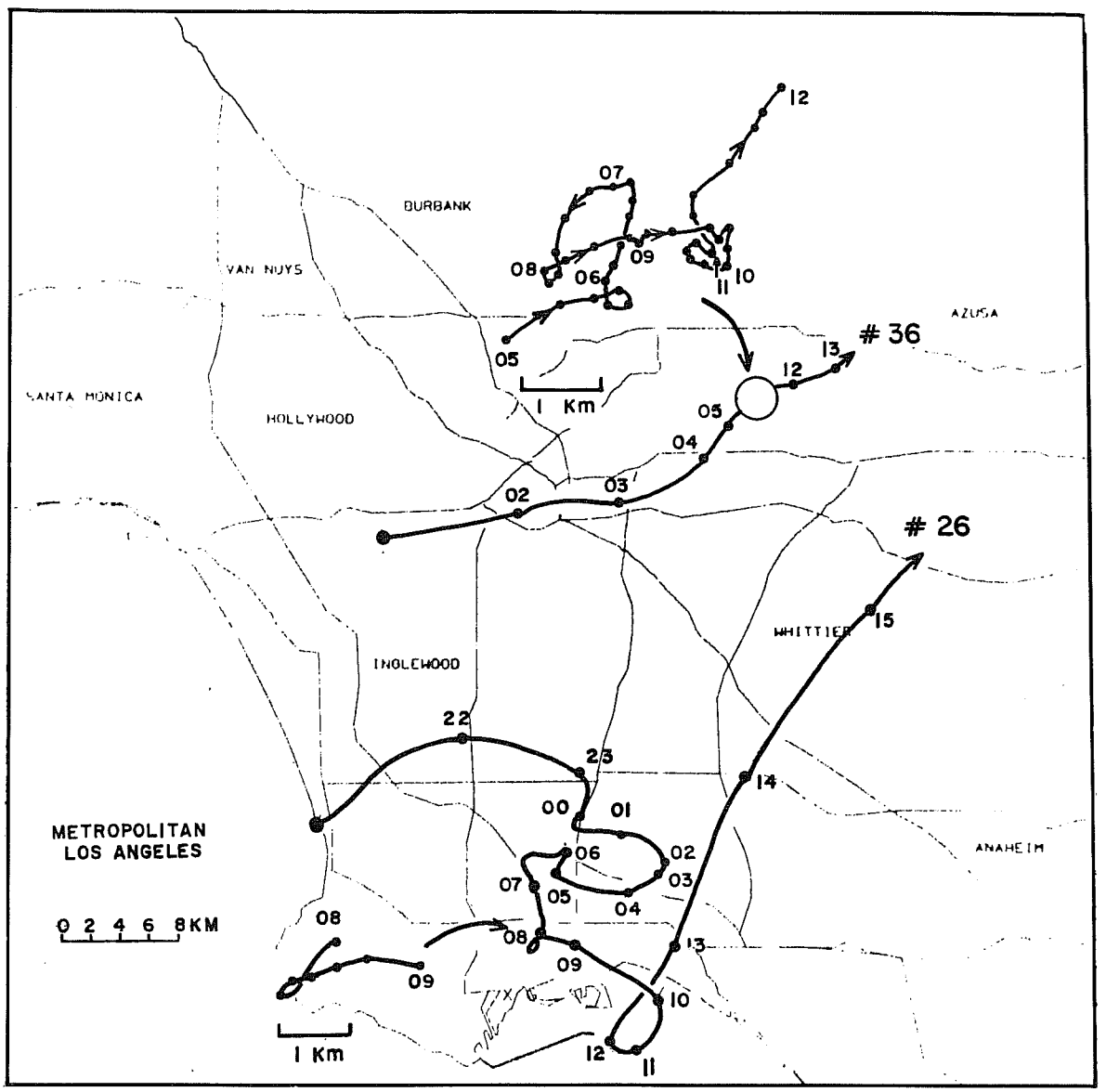

Figure 4. Examples of tetroon flights exhibiting stagnation and near-stagnation conditions. The trajectory segments have been expanded in scale by a factor of five. Numbers along trajectory are time (PDT).

26 exhibits seiche-like eastward and westward movements superimposed on a slow southward drift during the night. Near noon this flight traces out an anticyclonic loop over Long Beach Harbor before moving onshore in the sea breeze.

Surface air trajectories derived from the surface wind field within the Basin have been obtained by the Air Resources Field Research Office, Idaho Falls (see sect. 2.3), using data from a network of wind stations operated by the Los Angeles Air Pollution Control District, the National Weather Service, Federal Aviation Administration, and Department of Defense. The bottom diagram of figure 5 shows the mean vector comparison between many surface and tetroon trajectories initiated at the same point at the same time during the day (0900-2100 PDT) and at night (2100-0900 PDT). During the day there is very little systematic difference between the trajectories, but during the night the tetroon trajectories are directed to the left of the surface trajectory as they move downwind, presumably reflecting a systematic wind direction shear with height. The top diagrams show the average separation distance between surface and tetroon trajectories as a function of travel distance averages about 0.2 during the day and 0.5 at night. It is interesting that ratios between 0.2 to 0.3 have been obtained on the synoptic scale in the upper troposphere from comparisons of constant level balloon trajectories and trajectories derived from the pressure field and the wind field. The tetroon data were also analyzed to determine average wind speed, rms vertical velocity, and turbulence intensity as a function of time of day, as shown in figure 6. It is apparent that the maximum in average turbulence intensity occurs about 1000 PDT, although the maximum rms vertical motions are during midafternoon near the time of maximum temperature. Figure 6 shows that this is due to the forenoon minimum in the horizontal wind speed that occurs before the onset of the sea breeze. The minimum turbulence intensity is just before sunset, not at night, and is produced by the combination of continuing strong horizontal wind speeds in the sea breeze flow together with a rapid reduction in vertical motion after the time of maximum temperature. This phenomenon has interesting implications for the diurnal variability in concentration of a pollutant. Taken literally, it implies that for a constant emission of nonreacting material, the concentration could be higher just before sundown than at night. This possibility cannot be verified with air quality data available to us, because the oxidant type of data are too dependant on the photochemical process and on the nonuniform source emissions due to rush hour.

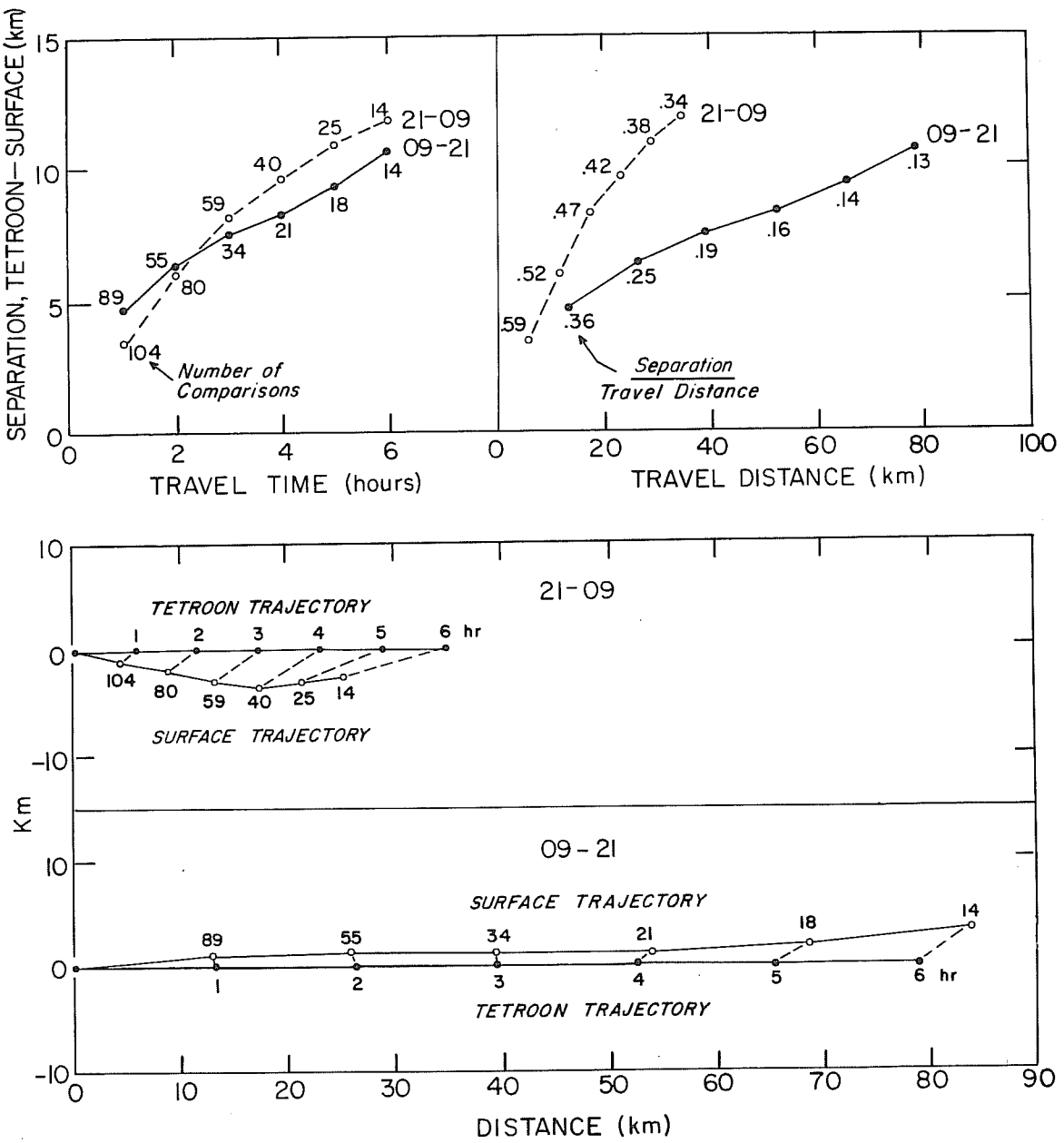

Figure 5. Average distance between tetroon and surface trajectories as a function of travel time and distance during the day (0900-2100) and at night (2100-0900) and the average vectorial difference in trajectories as a function of time and distance during day and night (bottom panel).

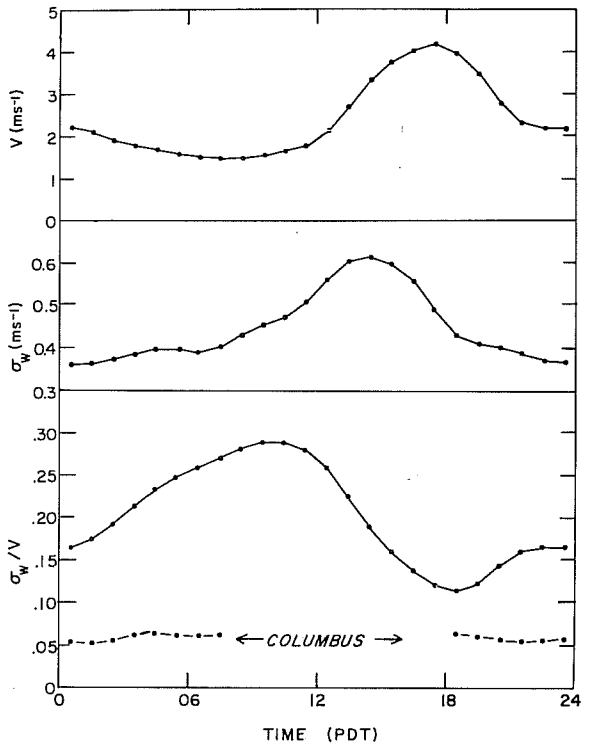

Figure 6. Average values of wind speed (V), rms vertical velocity (σ_w), and turbulence intensity (σ_w/V) as a function of time of day in the Los Angeles Basin. The dashed curve of turbulence intensity represents the nighttime data from Columbus, Ohio, for March 1969.

The bottom curve of figure 6 shows the tetroon-derived turbulence intensity data obtained over Columbus, Ohio, in March 1969. These data were confined to the nighttime hours. The Columbus values are smaller than the Los Angeles values by a factor of about 3 for the same times of day. This is attributed to the existence of strong thermal stability at Columbus with the resultant lack of significant vertical motion. There is the implication that the marine layer over the Los Angeles Basin at this time was not nearly as stable as the night inversion over Columbus. But whether this is caused by the moist marine air tending to produce a near wet adiabatic lapse rate, or whether this results from a large-scale "heat-island" phenomenon due to an almost complete coverage of the Basin by buildings cannot be determined from these data.

A helicopter followed the tetroons measuring oxidant concentration. Ozone values in the boxes along the flight path, as shown in figure 7, show how the ozone increases as the air flows northeast from downtown Los Angeles during morning and early afternoon. In general, ozone values close to zero in the downtown area near sun-up increase to values exceeding 10 pphm as the air moves into the Pasadena area about noon. The change in oxidant value along the tetroon track should be independent of advective influences and thus represents the temporal change due to photochemical reactions on the oxidant precursors. For comparison, local changes in ozone near the surface at El Monte are presented in the large boxes in figure 7. These local changes, of course, include effects caused by advection by the wind of already formed oxidants from other locations. At El Monte, the ozone increases until about 1500 PDT, then the arrival of the sea breeze brings about a decrease in ozone.

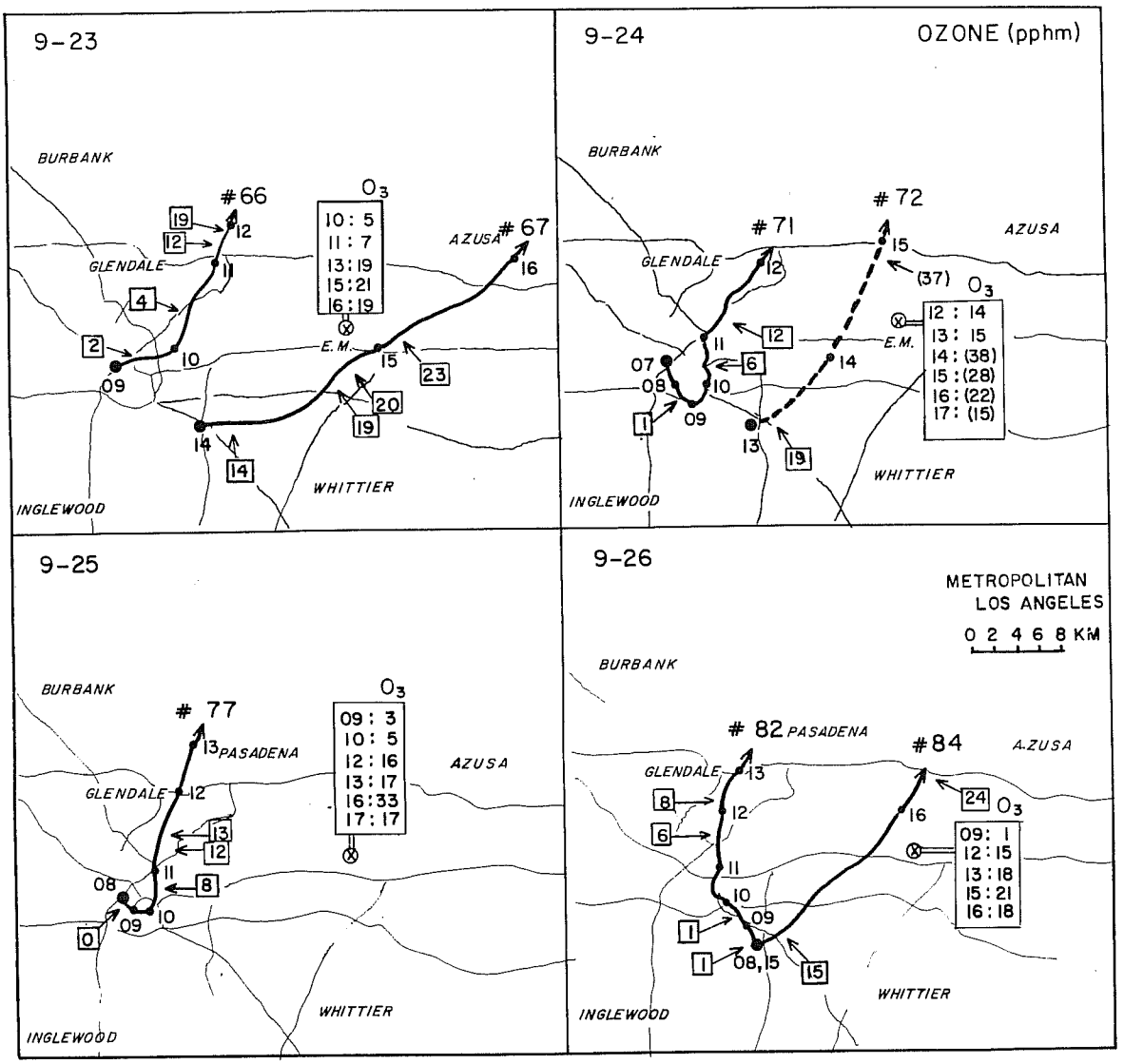

Figure 7. Changes in ozone (pphm) following the tetroon trajectories (boxed numbers) compared with the local changes at El Monte (large boxes). Unboxed numbers along the trajectories and the left-hand numbers in the El Monte boxes are time (PDT).

Note that both the oxidant following the tetroon and the oxidant at a fixed point should be influenced by variations in source strength with time, since, for example, the El Monte data can be affected by rush hour traffic, and the values along the tetroon path can also be influenced by material added by the traffic and mixed upwards into the original material.

1.2 Planetary Boundary Layer Dynamics

The data from an experiment in June 1970 (NOAA Tech. Memo. ERL ARL-28, 1971), in which wind profiles determined from a large number of double-theodolite pibal soundings near a 500 m tower were compared with profiles determined from anemometers mounted on the tower, failed to satisfactorily resolve the question of whether pibal winds agreed with winds measured using fixed instruments due to system problems affecting the tower instrumentation. A repetition of this experiment is planned for the coming fall. The data that are available, however, seem to indicate that pibal wind speeds are consistently higher than tower wind speeds (see fig. 8). This is consistent with measurements previously reported by Rider and Armendariz (1966). No obvious explanation for this phenomenon is available, nor is it yet certain that it is not due to some error, as yet undetected, in the measurement system. However, a computer model of balloon motion suggests that in a region of wind shear, a lighter-than-air balloon will always tend to indicate wind speeds faster than actually occurring, because the balloon, being less dense than the air, over-reacts to the accelerating force it experiences as it rises through a layer of increasing wind speed. An attempt will be made to test this model in the forthcoming experiment.

1.3 Energy Profiles of Small-Scale Wind Fluctuations

1.3.1 Turbulent Kinetic Energy Dissipation Rate

The continuing search for a general turbulence parameter, which will describe atmospheric diffusion over a wide range of scales, has led to some new and interesting models. One such parameter, the rate of dissipation of turbulent kinetic energy, is being applied with increased frequency to diffusion models. In addition to being an important term in the kinetic energy budget of the atmosphere, the dissipation also represents the rate of transfer of energy from the larger "energy-feeding" eddies to the smaller scale motion where it is dissipated into heat. Some recent applications include the large-scale diffusion model of Crawford (1966), and a general application in which Hanna (1968) suggested that the eddy diffusion coefficient can be expressed as a power law with a length scale and dissipation. Briggs (1969) dicusses the use of the dissipation to measure the rate of entrainment at the edge of a plume and thus as a mechanism that controls plume rise.

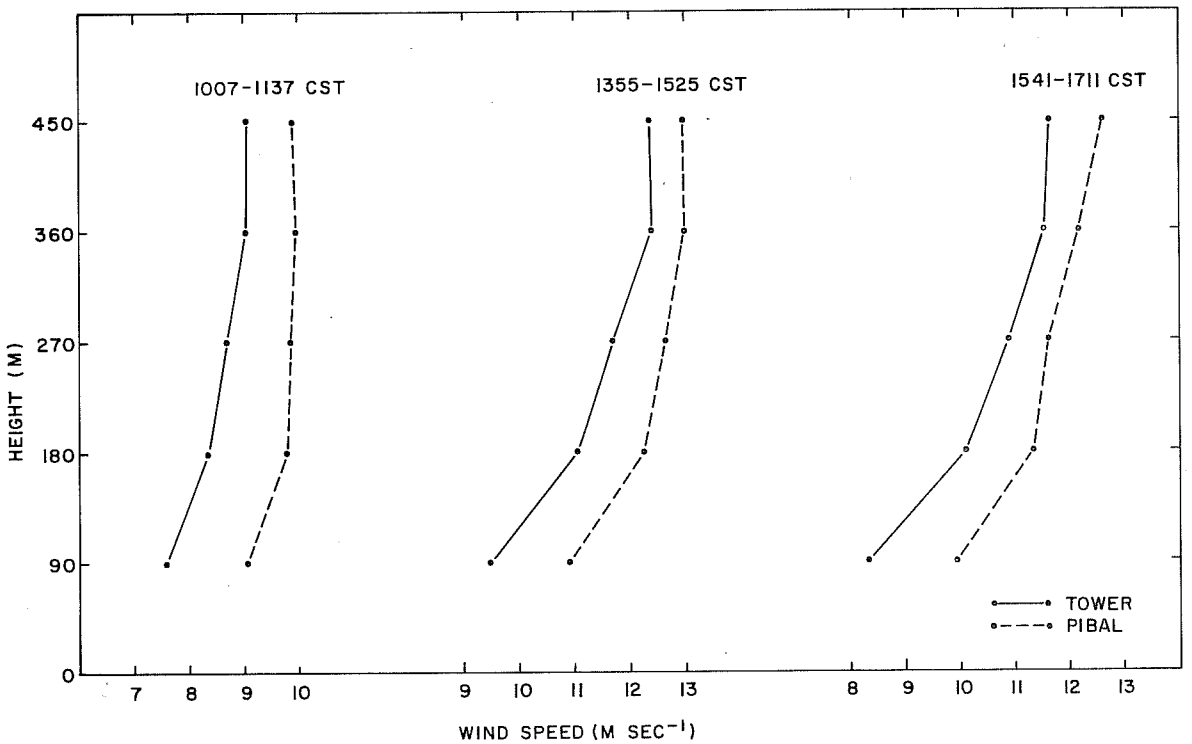

Figure 8. Comparison of wind speed profiles determined from tower instruments and double-theodolite pibal soundings for three 90-min periods on June 8, 1970.

1.3.2 Measurements

By means of a small aircraft, the Piper Comanche pictured in figure 9, estimates of the rate of kinetic energy dissipation were recorded from the surface to altitudes of 3 km. The variance of the indicated airspeed fluctuations, limited to wave-scales within the inertial subrange by a bandpass filter, was scaled to give a smoothed (time constant approximately 3 sec), continuous record of dissipation. All such data were processed through the Universal Indicated Turbulence System (UITS)[1] as described by MacCready et al. (1965) and MacCready (1966). This computer operates on the electrical signal from

[1]The UITS was developed by Meteorology Research Inc. (Altadena, Calif.), the initial unit under NASA Contract NAS4-784. Subsequently, military specifications were met and the unit was tested under Air Force Contract F19628-68-C-0229 and renamed the Air Turbulence Measurement Set (ATMS, AN/AMQ-26).

Figure 9. A platinum-wire thermometer and the pitot-static tube sensor to the UITS are mounted on the left wingtip of the Piper Comanche (260B).

a differential pressure transducer, which in turn represents impact pressure fluctuation from a wingtip-mounted pitot-static tube (see the left wingtip in fig. 9). Analog techniques were used to scale the transducer voltage to compensate for the power-law relationship between indicated airspeed and impact pressure and to remove the mean. The signal was then bandpass-filtered (-3 dB points at 7 and 12 Hz) to limit the effect of aircraft maneuvering, and engine vibration on the output. At low airspeeds ($\sim$50 m sec^{-1}) the fluctuations are confined to scales within the inertial subrange. An absolute value and a lag circuit are used in the last stage to approximate the variance. The output of the UITS is in terms of the "indicated turbulence" $(\rho\varepsilon/\rho_0)^{1/3}$, where ρ/ρ_0 is in the ratio of air density at flight altitude to that at the surface. While $(\rho\varepsilon/\rho_0)^{1/3}$ varies by an order of magnitude or more in the lowest 3 km, the ratio $(\rho/\rho_0)^{1/3}$ changes by only 20 percent in the extreme (at 3 km). Therefore, compensation is not made for these relatively small changes, and all results are presented in terms of indicated turbulence $(\rho\varepsilon/\rho_0)^{1/3}$ in $cm^{2/3}sec^{-1}$, which for the sake of convenience will be

represented by R. Measurements of the total air temperature, static pressure, and vertical acceleration were also recorded during each flight.

Interpretation of the "indicated turbulence" measurements in terms of the rate of dissipation of turbulent kinetic energy is predicated on the validity of the assumption that the flow is locally isotropic and that the measured fluctuations represent the u-component. In addition to isotropy, a fixed value is assumed to represent the "universal constant," b, in Kolmogorov's law,

$$S(k) = b\ \varepsilon^{2/3}\ k^{-5/3}\ , \qquad (1)$$

where S(k) is the one-dimensional longitudinal spectra at wave number k, and ε is the rate of dissipation of turbulent kinetic energy.

In addition to the standard, laboratory-type calibrations of the UITS computer, a series of level flights past a free-standing tower having a vertically oriented sonic anemometer; see Herbert (1970) for the details of this comparison. The results of 10 aircraft-tower comparisons are presented in figure 10. While the average value, as measured with the aircraft system, exceeds that measured on the tower, the difference is only 6.4 percent. The correlation between the two measurements is 0.9, and in all cases the difference between the aircraft and anemometer-derived dissipation is within ±10 percent of the measured value, thus within the specification limits of the analog computer.

The data used in this study were recorded during daylight (0845 to 1545 PST) in a 3-month period beginning April 1, 1970. All soundings were conducted near the Municipal Airport at Pendleton, Oregon. In most cases, the recordings were made while the aircraft descended in a linear or step-wise fashion; thus, the top of the mixed layer was selected as the lowest altitude where R represents the ambient conditions above. Normally this level corresponded to the top of the stable layer or temperature inversion that caps the mixed layer. Variations in both the temperature and indicated turbulence are less at this level than they are at the base of the layer. Becuase the stable layers are generally less than 50 m thick, the difference between using this method as compared with the conventional system, using the base of the layer, is small compared with the average mixing depth of 1.6 km (mixing depths ranged from 0.8 to 2.7 km).

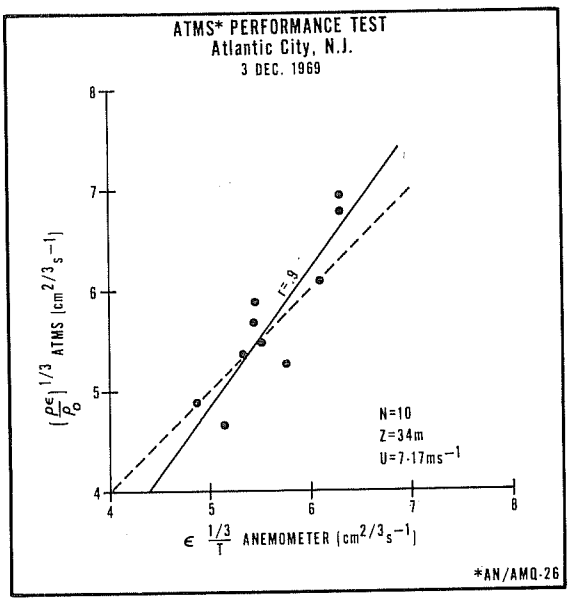

Figure 10. The results of 10 comparisons between dissipation estimates from a tower mounted anemometer and the UITS. Dashed line is the one-to-one ratio.

1.3.3 Rawinsonde/Aircraft Comparisons

On selected days throughout the project, rawinsondes were launched within 2 hours of an aircraft sounding. Comparison of the temperature and indicated dissipation profile with the temperature profile from a conventional rawinsonde illustrates some of the difficulties that may be encountered when using rawinsonde data to determine mixing depths. For the soundings on April 1, 1970 (fig. 11), the aircraft flight began almost 2 hours after the rawinsonde. Temperatures in the first 1.5 km had increased by about 2.5°C during this period, little change was observed at or above the inversion (1.8 km). During the interval, the mixing depth appears to have increased by approximately 0.3 km. The height distribution of R is typical of near-neutral conditions (strong wind throughout the layer associated with clear skies), in that there is a rapid decrease in R in the super-adiabatic sublayer from the surface to about 200 m with a more gradual decrease to values near unity at the base of the inversion. Values of R from the relatively turbulent-free air above the inversion are typically less than 1 $cm^{2/3}$ sec^{-1}. In the second comparison on April 17, 1970 (fig. 12), the launch time of the rawinsonde preceeded the aircraft sounding by only 14 min, and with clear skies and light winds the general situation is more unstable than in the earlier comparison. While there is a general decrease in R in the first 400 m, the gradient throughout the mixed boundary layer (height 1.4 km) is less than in the previous comparison. Nonetheless, the discontinuity at the top of the layer is well marked with an order of magnitude decrease. The temperature profile, as measured with the airborne thermometer, indicates weak stable layer at this level; this layer was not observed by the rawinsonde. In this situation, the rawinsonde would be interpreted to indicate the mixing to extend 1.2 km in excess of the actual depth. Clearly, the measured values of R are a much more sensitive indicator of the vertical extent of surface mixed layer than the temperature profiles.

1.3.4 Vertical Distribution of Dissipation

Figure 13 shows the ensemble averages of measured values of R from all flights plotted at 19 height increments that are uniform increments of the mixing depth, h. Where a linear-descent flight mode was used, the measured values are 30-sec averages. For step-soundings, the record was averaged for the duration of the steps -3 min. The bars at each level show the maximum and minimum individual values in the ensemble records. These values clearly depict the variation in R caused, in part, by altitude variations and intermittency in atmospheric turbulence at small scales. Such variations limit the interpretive value of a single sounding in the planetary layer.

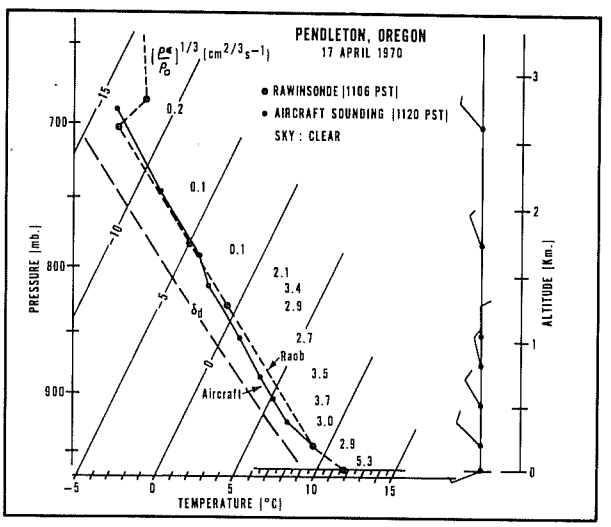

Figure 12. Comparisons of temperature profiles as measured on April 17, 1970, with a rawinsonde and the airborne instrumentation. The Skew-T log-P diagram is used.

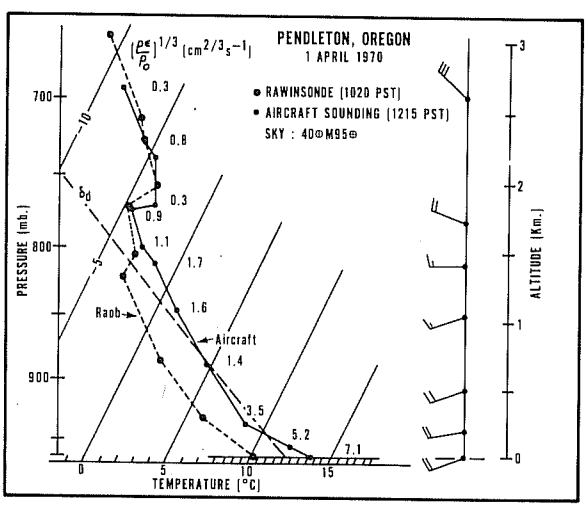

Figure 11. Comparisons of temperature profiles as measured on April 1, 1970, with a rawinsonde and the airborne instrumentation. The Skew-T log-P diagram is used.

Due in large part to the variations in the temperature soundings and the absence of detailed wind profiles, it was impossible to classify individual soundings according to normal stability criterion. Nevertheless, the lower portion of all soundings in the spring was unstable. The airport weather observations (cloud cover and surface wind speed) were used to separate the four most unstable soundings (minimum cloud cover, winds less than 3 m sec^{-1}) and four near-neutral soundings (low overcast and strong surface winds) from the total set. The average dissipation profile for these two cases is shown in the two left-hand panels of figure 13. In both

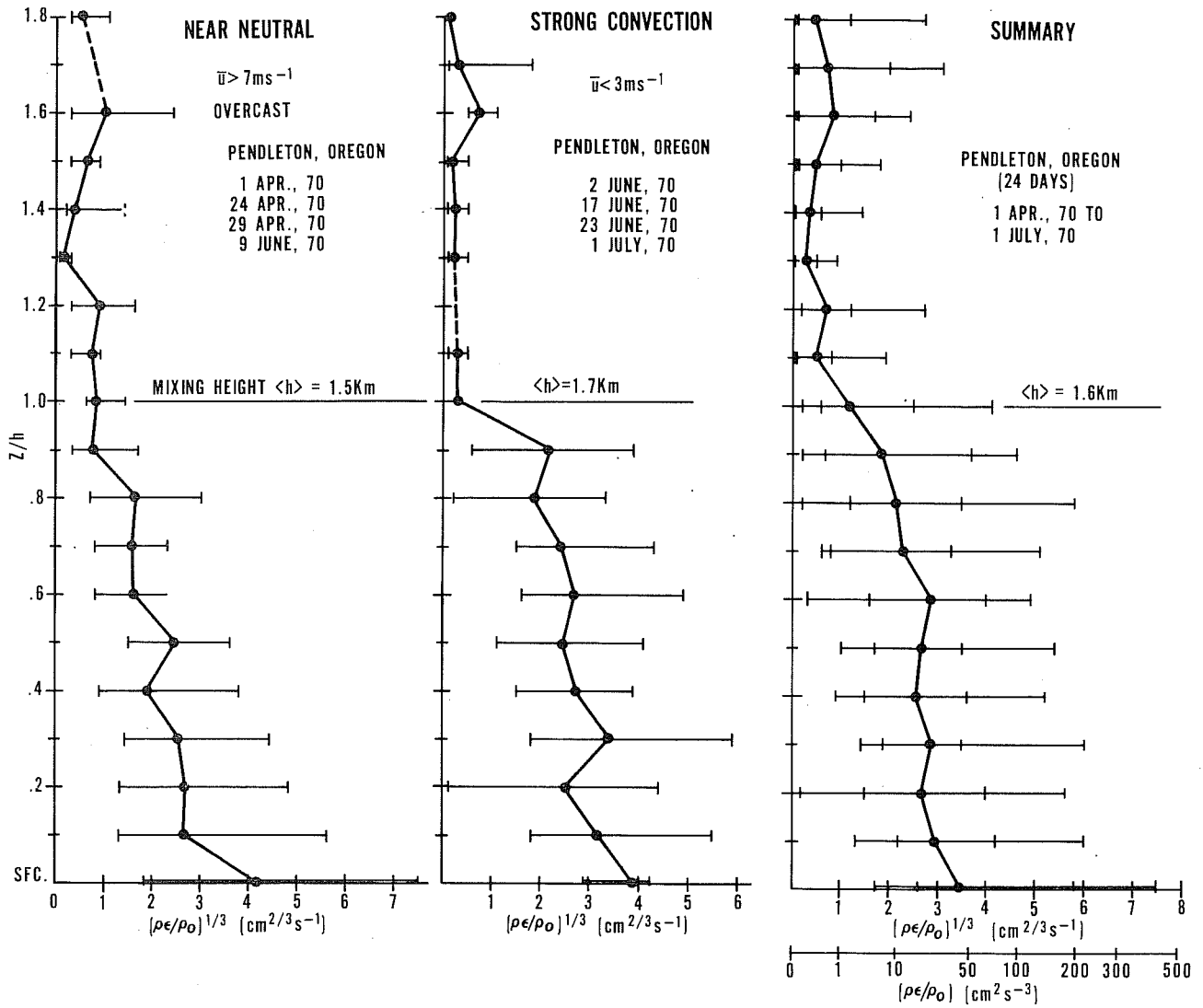

Figure 13. Summary of the distribution of $(\rho\varepsilon/\rho_0)^{1/3}$ *with height (z) normalized by the mixing depth (h).*

cases, there is a general decrease of R with height, but the decrease is more gradual in the unstable case than in near-neutral conditions. Variations in R, as indicated by the bar lines, are also greater during strong-convection. The decrease from the surface R = 3.8 to R = 2.4 at top of the layer with an abrupt decrease through the stable layer to R = 0.2 is very similar to the dissipation soundings reported by Volkov et al. (1968) over the Steppes on slightly cloudy days. The average of nine aircraft flights showed a value for $\varepsilon^{1/3}$ of 4.5, 2.3, and 1.3 $cm^{2/3}$ sec^{-1} at 60, 900, and 1200 m, respectively. Readings and Rayment (1969) discuss similar variations in the gradient of ε, measured with balloon-borne anemometry at Cardington, England. In the data that correspond to the near-neutral case (mean net surface radiation less than 12.5 mW cm^{-2}) decreases as z^{-1}. In more convective cases (mean net radiation in excess of 12.5 mW cm^{-2}) a more gradual decrease with height is observed. Readings and Rayment attribute the difference to the production of energy by buoyancy at greater heights in the high radiation conditions. One feature of the variation of dissipation with height is common to all three data sets, that is, the increase in variability at the base of the inversion that caps the mixed layer.

In the third panel on the right of figure 13, the results of all flights are summarized. The inner bars now indicate the range of the mean values observed at each level. In the mean the ε values decrease with altitude from 200 cm^2 sec^{-3} at the surface to less than 0.1 cm^2 sec^{-3} in the region immediately above the planetary boundary layer. The variation about the mixed layer are generally measured in cloudy air.

2. RESEARCH AT THE NATIONAL REACTOR TESTING STATION, IDAHO

2.1 Building Wake Turbulence and Diffusion

The effect of building structures upon downwind diffusion rates has been examined theoretically (in very simplified manners), in wind tunnels, and in very limited instances by full scale measurements in the atmosphere. Little knowledge exists about the effect of structures during temperature inversion conditions and very light, meandering winds. Practical information is needed about both the magnitude of this effect and the conditions (building size, minimum wind speed, etc.) during which building wake effects vanish. To answer some of these questions, we erected a simple cubical stack (8 m on a

side) of hay and straw (a cheap way to fabricate a semichangeable structure) at the apex of the diffusion Grid III. Bidirectional vanes, cup anemometers, and temperature sensors were placed upgrid and downgrid of the structure to observe longitudinal and vertical profiles of wind and temperature. The basic field testing program is the following. Downwind effluent concentrations are measured directly and compared with the diffusion climatology of the test grid developed in previous years. From these direct measurements, the magnitude and downwind extent of the structure influence are determined.

A number of field measurements using uranine dye effluent and meteorological instrumentation have been performed. Detailed examination of the bivane wind fluctuation data revealed that some vanes developed excessive frictional drag during meteorological instrumentation tests. A modification of the bivane slip-ring brushes has been developed and installed in the vanes. The excessive frictional drag has been eliminated, and this type of data will be collected in forthcoming testing. A limited amount of data free of frictional influences suggested that the 8 m^3 is too small to yield significant wake influence on diffusing effluents during very low wind speeds. To determine if this structure produces wake diffusion effects, we made a few releases of uranine dye. The interpretation of the tests conducted to date is that the structure is of marginal size to generate significant effects upon either meteorological instrumentation or diffusing effluent plumes. The structure is being enlarged, and the full range of testing will resume shortly.

The field testing site consists of two sampling grids with a common apex. The 8 m^3 structure is centered at the apex. One sampling grid is within a sector 80 degrees wide and opens toward the northeast. The second, and new, sampling grid is 120 degrees wide and opens toward the south-southwest. High volume air samplers are positioned on arcs at 4 degree intervals at 1 m above the ground. Each grid has sampling arcs at radial distances of 25, 50, 100, 200, and 400 m. Vertical samples are available at 4, 8, and 12 m above the ground ($\frac{1}{2}$, 1, and $1\frac{1}{2}$ building heights) at positions on the 25-, 50-, and 100-m arcs. Seven vertical sampling profiels are available at the 25-m arc, covering a lateral span of 60 degrees. At 50 and 100 m downwind, single vertical sampling profiles are measured downgrid from the central vertical sample profile on the 25-m arc (the centerline established for the sampling grid).

Bidirectional vanes, cup anemometers, and temperature sensors are positioned along the same grid centerlines (one centerline for each sampling grid). Bivanes and cup anemometers are mounted 4 m above the ground at 200 m upwind and at 17, 50, 100, 200, and 400 m downwind of the haystack center. Temperatures are measured at 1, 2, and 4 m above the ground at both 17 m upwind and downwind of the stack center.

The 61-m Grid III tower lies along the 200-m arc to the southwest of the apex. Temperatures and wind speeds are measured up the tower to document the general conditions during testing. Wind speed profiles are determined from cups at 1, 4, 8, 16, 32, and 61 m above ground. Temperatures from 1, 2, 4, 8, 16, 32, and 61-m levels on the tower are recorded each minute. Wind speed profiles are measured along the sampling grid center lines (25, 50, and 100 m upwind and downwind) at 1, 4, and 8 m above ground.

Wind profiles are recorded on totalizers (counters), and as voltages on high speed digital systems. Temperature profiles from the 200-ft tower are digitally recorded on punched paper tape. Bidirectional vane readings and the adjoining wind speeds are recorded digitally on magnetic tape, once each second.

A uranine dye solution is dispensed under high pressure to generate a plume of small particulates, and the particles are collected on glass fiber filters at each high volume air sampler location. The dye loaded filters are washed in the laboratory by a metered amount of solution and the fluorescence per unit volume of the solutions are measured by a sensitive photoelectric detector. Average air concentrations are derived from the calibrated voltage meter readings and the total high volume air sampler flows during testing. The uranine dye tracer technique has been described in detail by Dumbauld (1962).

The data collected from the Grid III field test array show promise of providing useful information. An interpretation of the data collected to date will not be presented now since a larger data base is necessary. A brief discussion of dye test No. 2, conducted on May 12, 1971, is presented to illustrate some of the information and results expected from the program. The general conditions during testing are summarized in table 1.

The ground was dry during the uranine dye release. The state of the sky was 2/10 altocumulus with a few cirrus. Visibility was greater than 50 miles. The mean hourly temperature profiles from the Grid III tower from 0300 to 0900 MDT are shown in figure 14.

Table 1. Meteorological Conditions During Test No. 2.

5/12/71 (MDT)	Wind 4m	Temperatures (°F)					
		32m	16m	8m	4m	2m	1m
0615 to 0722	024° 2.2 m sec^{-1}	42.6	41.9	41.4	41.3	41.2	41.2

Uranine dye samples were collected on Grid B, the new grid extending toward the southwest. The NRTS stability category during sampling was between classes D and E. The stability category was determined by several means. A subjective means (Yanskey et al., 1966) was used in which the stability category was obtained from a table containing categories of solar insulation, wind speed, and cloud cover. An alternate technique of estimating stability category used bidirectional vane measured lateral wind direction fluctuations. The standard deviation of wind direction was substituted into a NRTS empirical equation to calculate σ_y, the standard deviation of lateral effluent concentration. This calculated value of σ_y was compared with NRTS climatological curves of σ_y for stability categories. The stability category could be inferred from the position of the calculated data point relative to the mean curves for the categories. Both techniques placed the stability category between classes D and E. The vertical temperature profile supported that finding. The mean profile was near isothermal in the first 8 m above the ground, and a weak inversion was between the 8 and 32 m levels (refer to table 1). The peak sampled dye concentrations and the open terrain climatological axial concentrations are plotted versus distance in figure 15.

The building dilution effect has developed by the time the plume reaches the 25-m sampling arc. Between 100 and 200 m downwind (12½ to 25 building reference lengths) the axial concentrations in the building wake decrease more slowly with distance than the open terrain rate of dilution with distance. For a mean wind speed of 2.2 m sec^{-1}, this rate of dilution change occurs at an Eulerian time of about 45 to 90 sec. For an assumed Lagrangian-Eulerian time scale on the order of $\beta = 4$, this test suggests that the plume may have "forgotten" the effect of the building after about 20 to 25 sec.

The example measurements show the development of building wake dilution and its apparent downwind extent. The continuing series of tests will examine the generality of these effects, the mean and extreme differences between

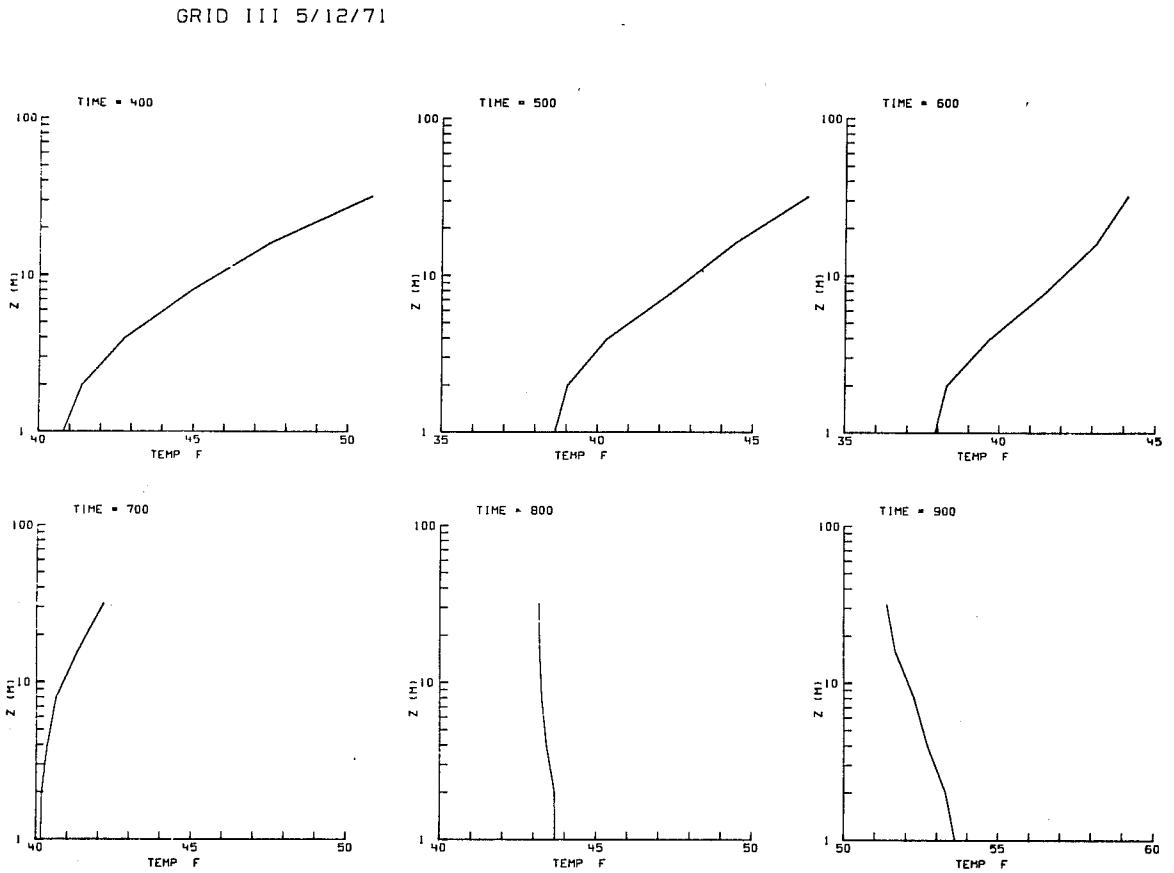

Figure 14. Mean hourly temperature profiles from Grid III tower for 0300-0900 MST 5/12/71. Tracer release occurred 0615 to 0722 MDT.

concentrations inside and outside of the wake, the downwind extent of the wake diffusing regimes, and the relationships between the size of the obstacle and meteorological conditions and either the distance or the time locations of transitions to successive diffusing regimes.

2.2 Mesoscale Transport and Dispersion Studies

2.2.1 Terrain Influence on Mesoscale Wind Fields

Since the research involving the network of wind towers over the Upper Snake River Plain began, several important features of the boundary layer mesoscale flow over this area

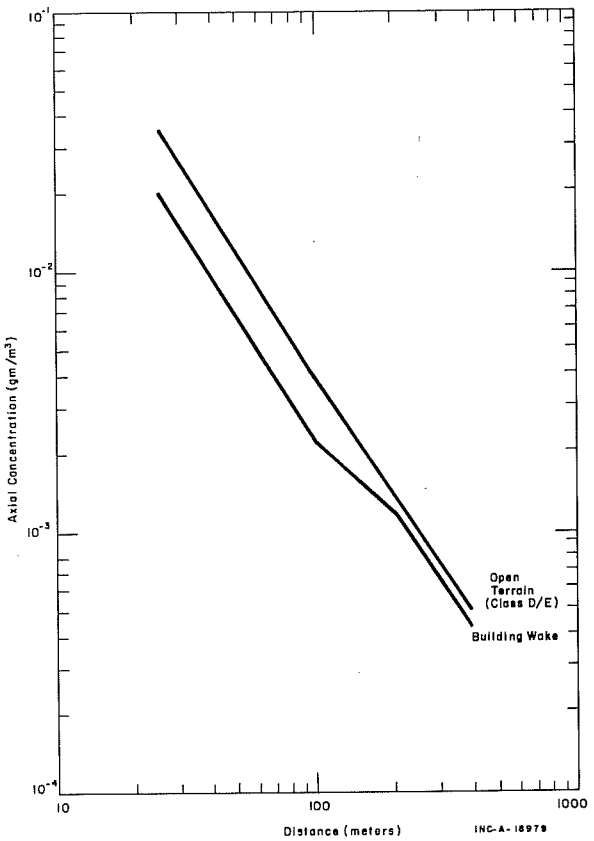

Figure 15. Building wake and open terrain axial concentrations vs. distance for dye test No. 2, May 12, 1971.

have been uncovered. Probably the most important discovery was that the representation of the wind by a single station, over more than a few miles, can often lead to serious errors in estimating atmospheric transport (NOAA Tech. Memo, ERL ARL-28, 1971). The examination of plots of selected wind fields and trajectory patterns indicated a variety of flow patterns and transport configurations (ESSA Tech. Memo, ERLTM-ARL 20, 1970). One of the more intriguing flow patterns was the recurrent formation of a large circular eddy in the upper portion of the computational grid.

The observation of this phenomenon led to a more careful examination of the rather mild topographic variation over the plain. This variation is indicated by the elevation contours shown in figure 16 with stippling over the area below 5000 ft. Probably the most striking feature is the interruption of the southwestward slope of the plain by the higher ground (above 5000 ft) jutting out from the mountains to the northwest. This creates a fishook-shaped depression that proceeds northeast along the Snake River up the right side of the grid, then northwest across the top of the grid, then southwest along the left side of the grid, and ends in the southern portion of the test site. The shape of the curved portion of this depression resembles the shapes of the eddies observed in several selected cases.

To establish a climatological estimate the importance of this topographic feature on the flow patterns over the area the 6 hourly windfield plots for all of 1969 were examined with the outline of the 5000-ft contour superimposed. We found that varying degrees of conformity of the wind to the topographic depression can be observed during about 57 percent of the time. This correlation varies from a high of 63 percent during the spring to a low of 42 percent during

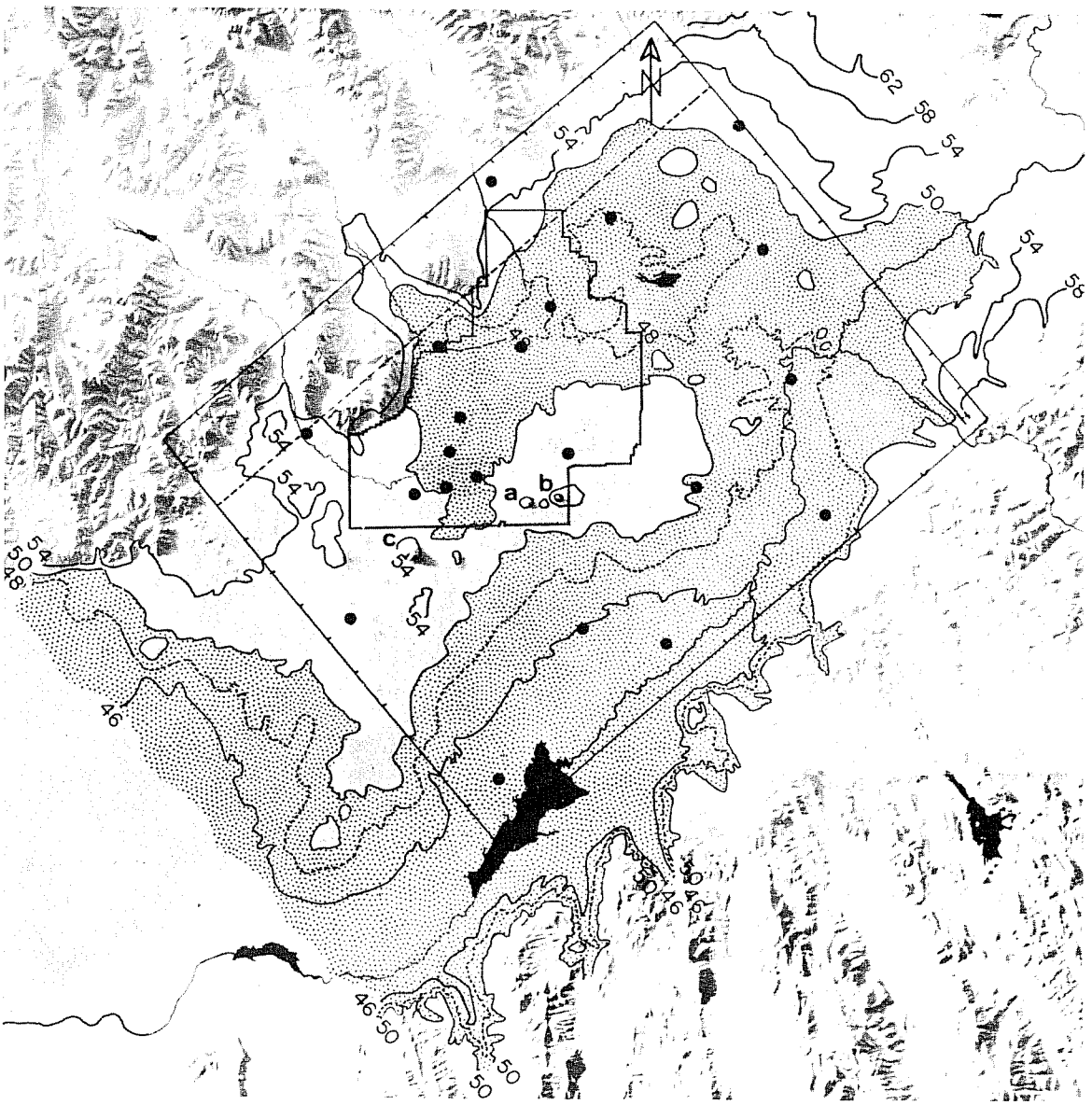

Figure 16. Relief map of the Upper Snake River Plain in southeastern Idaho. The values shown on the few contour lines over the plain are in hundreds of feet. The stippled area within and adjacent to the grid indicates the area below 5000 ft MSL. The tic marks along the border of the grid indicate the grid point separation, which is 5.33 miles.

the fall. Examples of this conformity are shown for the four seasons in figure 17. The definition of the symbols used in the plots is shown in table 2. In the absence of other dynamic effects, this type of flow might be expected to occur simply through the channeling of a light southwesterly flow entering the lower end of the plain. Another explanation of this phenomenon, at least during the warmer seasons, might be as follows. During synoptic conditions in which the pressure gradient over the area is weak and the major driving force for the air motion is gravity, daytime heating would cause the flow over the plain to be from the lower terrain southwest of the grid to the higher terrain northeast of the grid. As the cooling process begins in the evening, the tendency to reverse the direction of the flow along the top of the grid is much stronger on the northwestern half because of the steeper terrain in that area. Thus, the inertia of the southwesterly flow is overcome sooner in that area and the flow becomes northeasterly into the portion of the depression that extends southwest over the test site. This is probably not the only cause of the phenomenon, but we expect it to be a major one.

A further refinement of the phenomenon just described was observed to occur during about 12 percent of the days during 1969. This is the situation when the conditions are suitable for a circular shaped eddy forming in the upper portion of the grid and persisting for a few hours. A few examples of this eddy, one for each season, are shown in figure 18. This condition occurs primarily at night and most frequently during the summer. This would indicate that it is most closely, but not entirely, associated with the diurnal heating cycle and local topographic features.

The flow patterns just described are interesting because they are examples of organized spatial variations in the flow pattern. They would also be extremely difficult, it not impossible, to determine from wind rose plots at several locations. This type of spatial variation in the flow is very important because of its implications in the transport of material over the area.

The type of flow that can be represented easily by the winds at a single location does occur over the Upper Snake River Plain in the form of episodes of strong south-through-southwest flow or strong north-through northeast flow. The uniform flow with the strong (average greater than 10 m sec^{-1}) southerly component was observed during some portion of about 14 percent of the days in 1969. The uniform flow with the strong northerly component was observed about 7 percent of the days in 1969. Occasionally the south-through-southwest

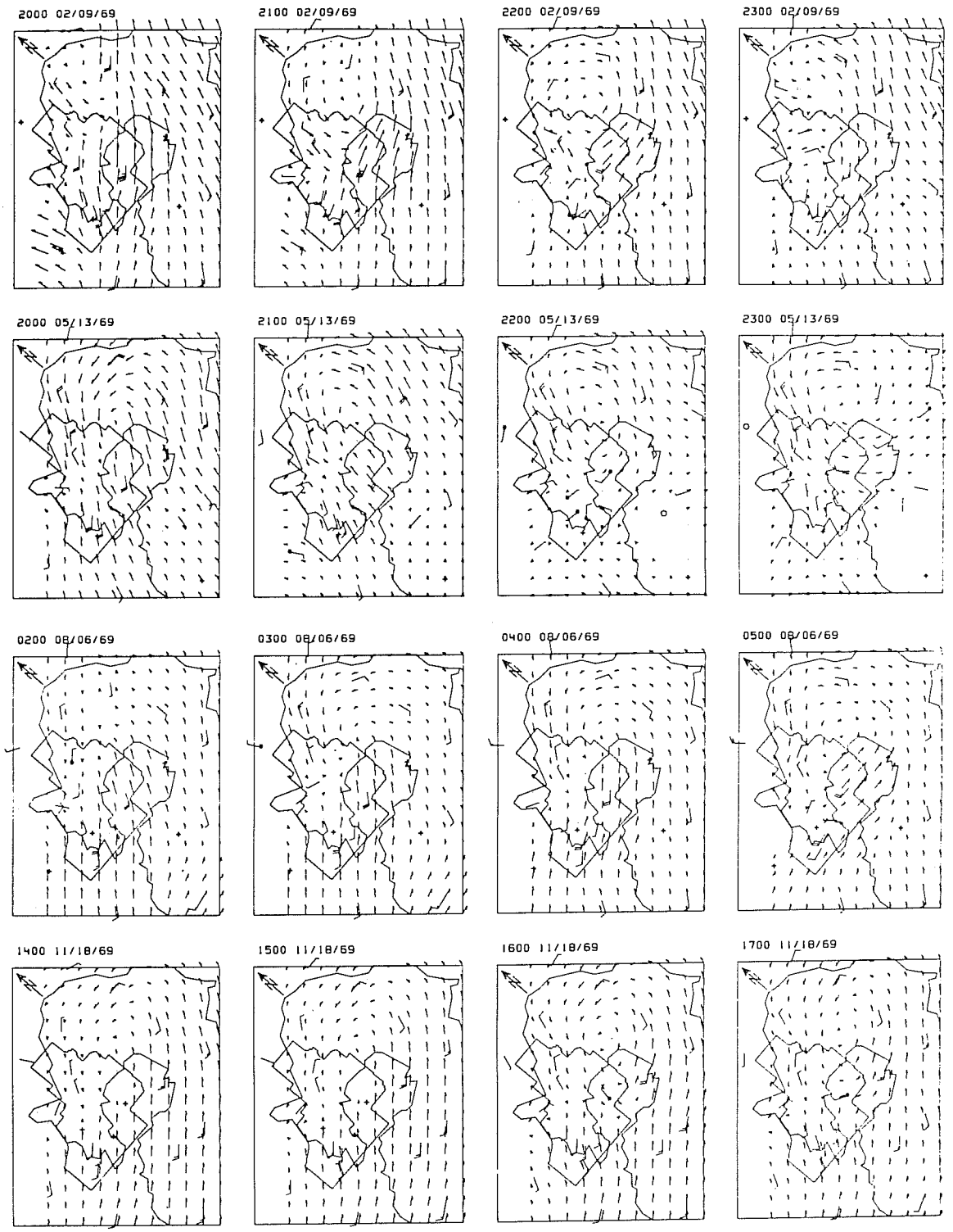

Figure 17. Examples of the flow pattern over the grid conforming to the topography. A 4-hour series is shown for each season. The 5000 ft contour is included for reference (see fig. 16). Wind data from each station are plotted in standard form, and the interpolated winds are plotted as vectors at each grid point (see table 2). Time (MST) and date are at the top of each plot.

Table 2. Definitions of Symbols.

Symbol	Definition
At Wind Stations	
Standard Shaft and Barb	Wind direction and speed (Each barb = 10 mph)
*	A direction change of 90° or greater during the averaging hour
+	Missing data
0	Calm
At Grid Points	
↽	Wind speed and direction. (Distance between grid points = 25 mph)
→	$2<\|V\|<5$ mph
-	$\|V\|<2$ mph
	Calm

winds were prefrontal and the north-through-northwest winds were post frontal, but in the majority of the cases they were both associated simply with strong pressure gradients. Examples of both of these types of flow are shown in figures 19 and 20.

Another characteristic of the flow that has been observed, but less frequently than any described previously, is channeled flow out of one or more of the three valleys northwest of the grid. Two examples of this are shown in figure 21. The sequence during the early morning of March is an example of a strong wind situation and the sequence during the late evening in November is an example of a light wind situation. A wind rose for the station in the valley northwest of the grid shows down-valley flow faster than 7 m sec^{-1} about 5 percent of the time. This indicates the relative infrequent occurrence of episodes showing a sustained effect, by this phenomenon, on the flow pattern over the plain.

Probably the most dramatic occurrence observed in the flow pattern is the passage of a definitive frontal system. In this case, as in the case of the sustained strong uniform winds over the grid, the effect of the relatively mild terrain variation over the grid is hardly discernable. One example of this phenomenon is shown in figure 22. The winds observed at 1300 MST, May 30, 1969, are from the southwest

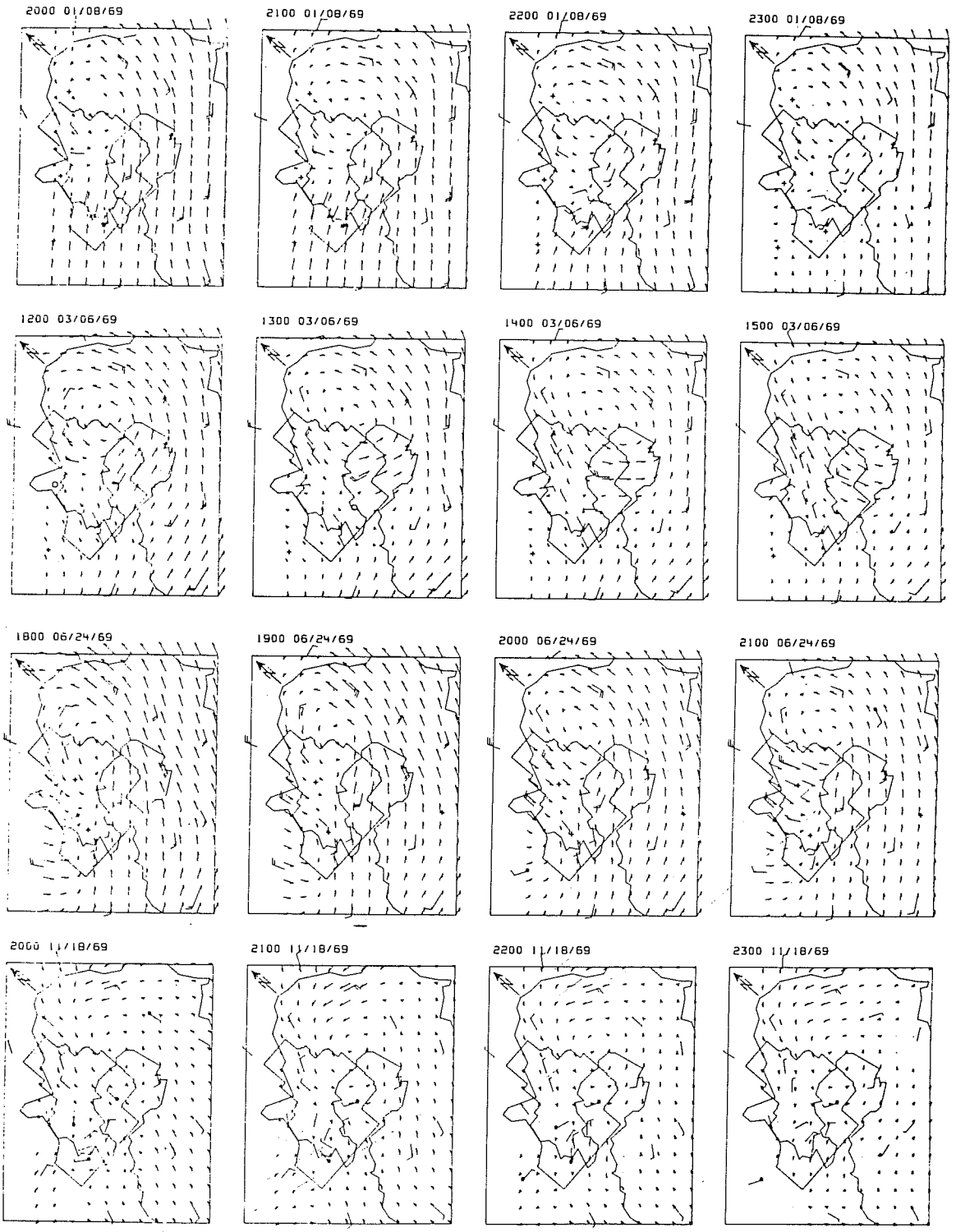

Figure 18. Examples of a cyclonic eddy in the upper portion of the grid. See figure 17 for other details.

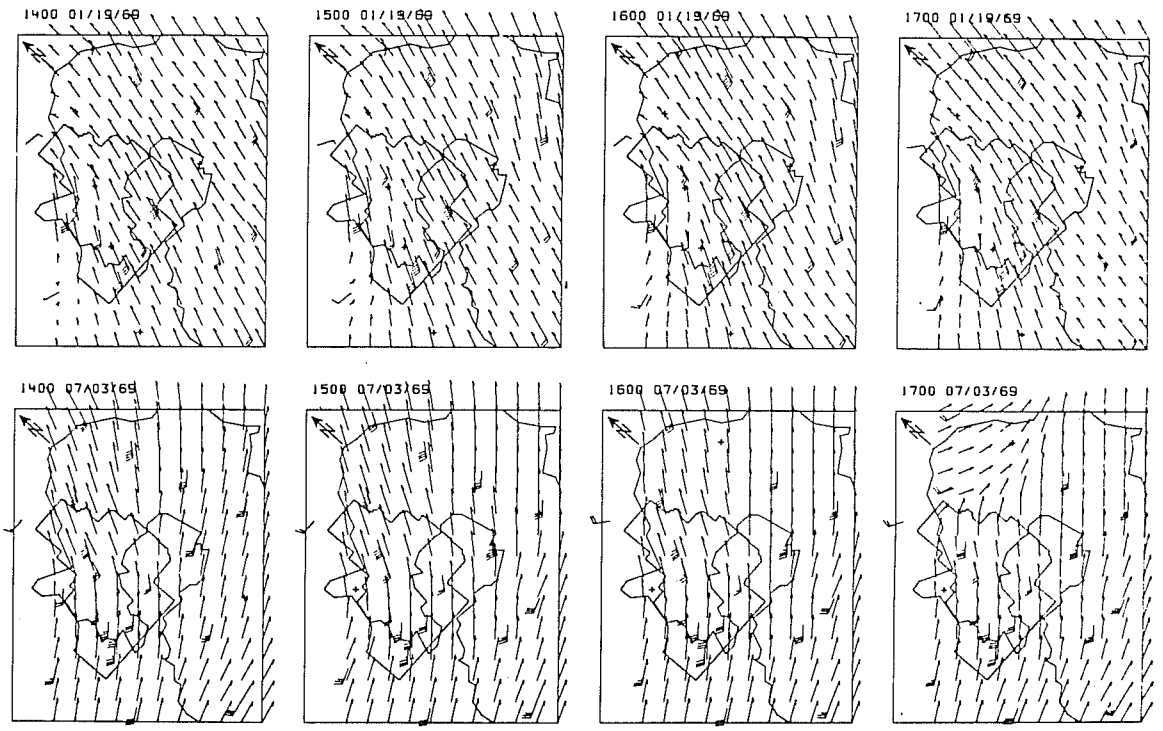

Figure 19. Examples of a strong sustained uniform flow with a large southerly component. See figure 17 for other details.

generally in excess of 13 m sec^{-1} over most of the grid. The station in the valley just north of the site boundaries gives the first indication of the approaching front, which then moves across the grid from the northwest in a matter of about 9 hours. There are weaker indications of frontal passages during the year, however. Those of the intensity of this example occur during about 3 percent of the days of the year with a high of around 7 percent in the spring.

The features in the flow patterns presented here illustrate that the expanded point of view provided by a display of a network of wind observations can be a valuable tool in studying mesoscale phenomena. The microfilm recording of cathode-ray tube plots makes the process economically feasible. The influence of the terrain features over the Upper Snake River Plain is quite evident in a sizeable percentage of the flow patterns observed. Information of this type is extremely valuable in determining transport conditions for a given area under various synoptic weather conditions. For a comparison, this kind of study should be carried out over an area with flat surrounding terrain.

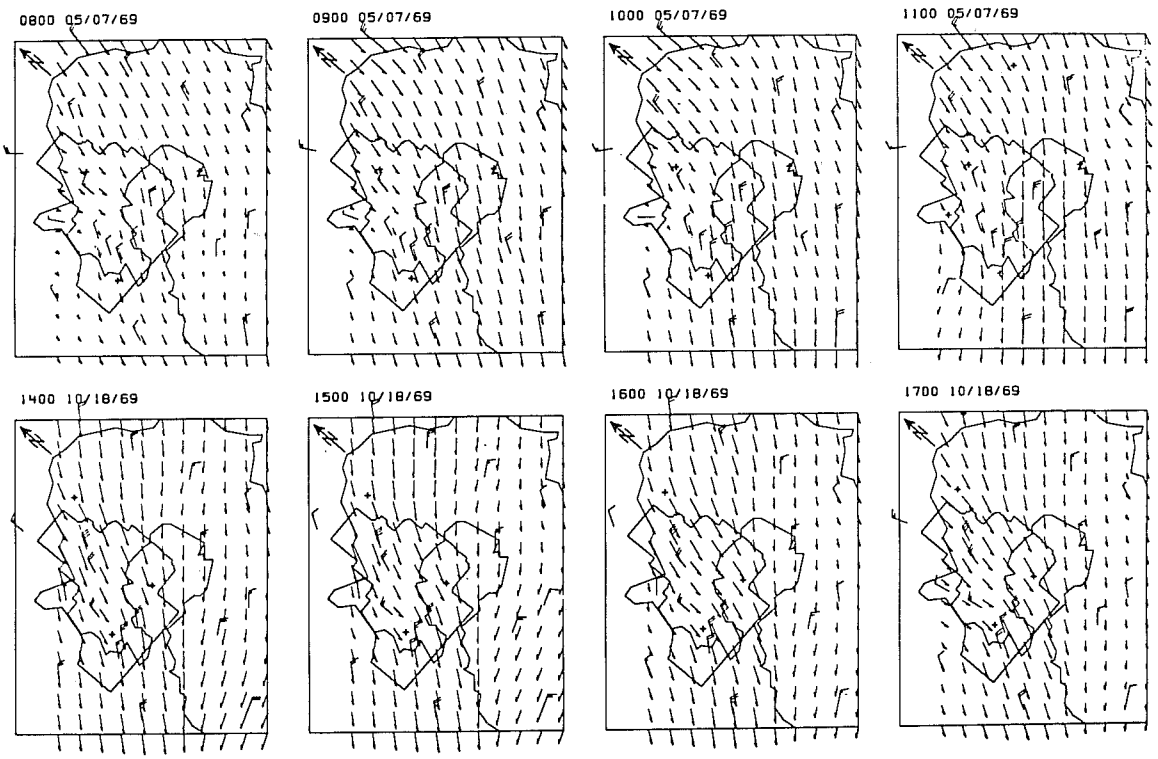

Figure 20. Examples of a strong sustained uniform flow with a large northerly component. See figure 17 for other details.

2.2.2 *Climatology of Wind Field Derived Mesoscale Trajectories*

One of the primary goals of this mesoscale wind research has always been to establish a climatology of transport from various locations at the National Reactor Testing Station (ESSA Tech. Memo ERLTM-ARL 20, 1970). To provide a preliminary data base for this project, wind-field derived trajectories of hypothetical particles, released one per hour from the same location, were plotted 12 to a diagram for all of 1969 (Wendell, 1970). Examination of this series of plots reveals a substantial variety of trajectory patterns. There are several cases, however, in which the patterns are similar enough to be recognized as relatively distinct types. A few of the more common types are shown in figure 23. The percentages of occurrence of these types were determined by subjective visual examination and are shown in table 3.

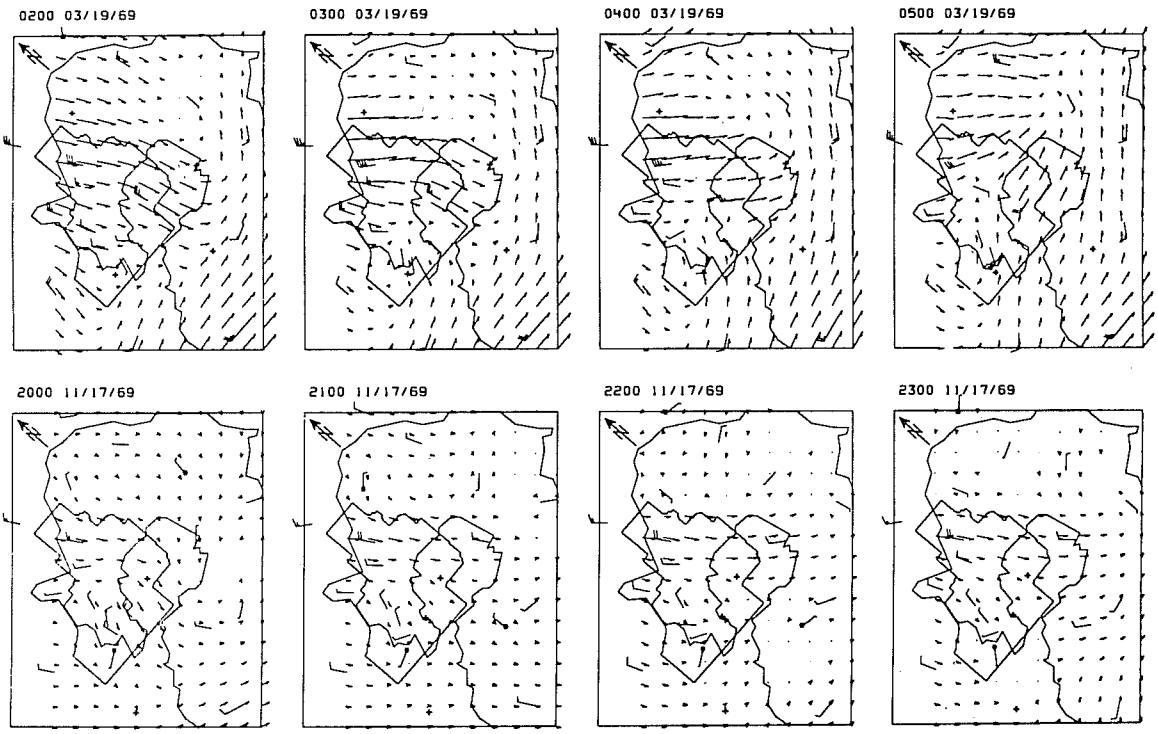

Figure 21. Examples of a valley wind extending significantly over the plain. See figure 17 for other details.

The most common pattern of trajectories for the entire year, regardless of release times, is designated as type "A" and is characterized by the fact that all 12 "particles" released move in a southwesterly direction with little deviation until they leave the bottom boundary of the computational grid. This indicates a sustained northeasterly flow from the source to the boundary at least for the duration of the release period. Considering the entire year, the variation in the percentages of occurrence is small enough to indicate very little preference for one release period or the other. This also seems to be true for each individual season, except winter, in which 0100-1200 MST release period holds a significant edge. This type of transport pattern is maximum in the winter and minimum in summer. In fact, this pattern predominantes each season except summer, when it ranks fourth and fifth for the 0100 and 1300 MST releases, respectively. During the winter season of 1969, this pattern persists for up to 8.5 days

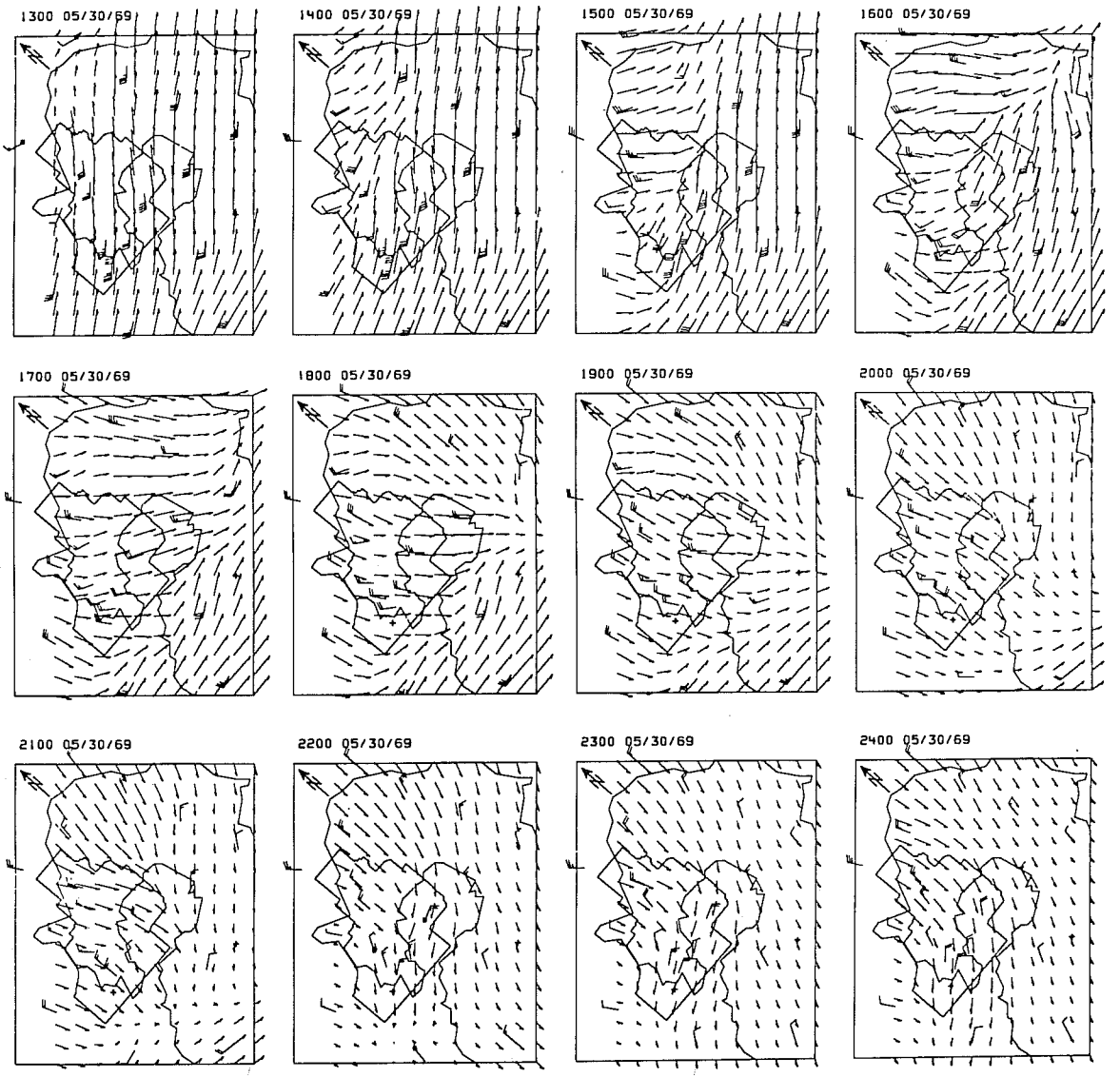

Figure 22. Example of the effect of a frontal passage on the flow pattern over the grid. See figure 17 for other details.

The next most persistent type on an annual basis is type "B" and is recognized by the steady northerly procession of particles directly off the left boundary of the grid. This would be caused by a sustained southerly flow lasting throughout the entire release period. This type shows, as did type A, no particular preference for either release period. This type occurs a maximum of 16 percent during the winter, and it ranks as the second most frequent type during this season.

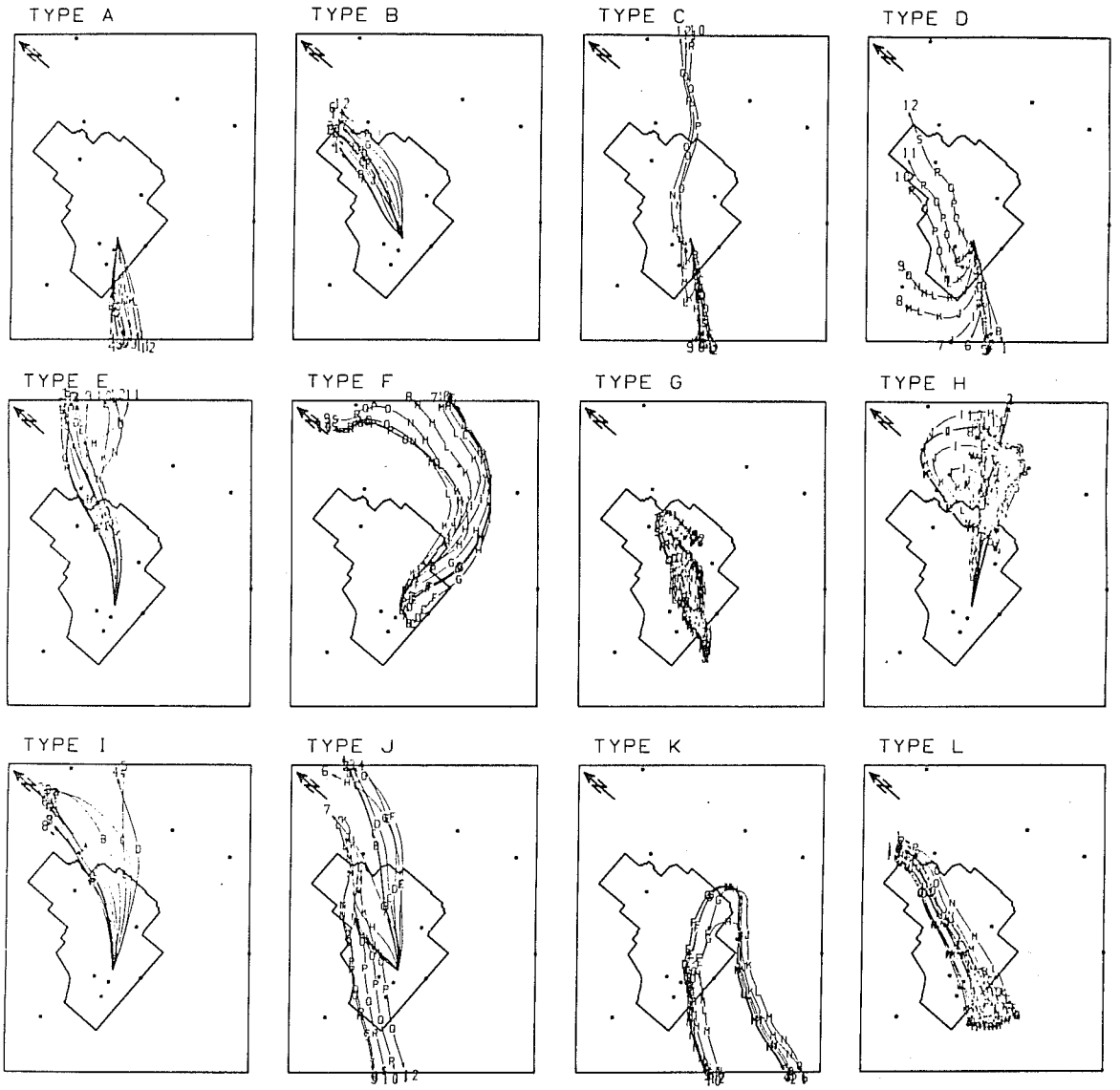

Figure 23. Trajectory patterns typed according to frequency of occurrence (see table 3).

The only other significant occurrence of this type is in the fall at 8 percent, and it ranks fourth and second for the 0100 and 1300 MST releases, respectively.

The third pattern designated type "C" is the first to indicate a change in the flow during the release period. The particles released at the beginning of the period move to the southwest and off the grid indicating several hours of northeasterly flow from the source to the bottom of the grid. During the release period, however, the direction of motion of

Table 3. Percentage of Occurrence of the Trajectory Pattern Types (Numbers in Parentheses) for the Year, Seasonally, and According to Release Period. Time in MST.

Type	Year		Winter		Spring		Summer		Autumn	
	0100 (%)	1300 (%)	0100 (%)	1300 (%)	0100 (%)	1300 (%)	0100 (%)	1300 (%)	0100 (%)	1300 (%)
A(20)	21	18	30	22	21	17	8	7	27	26
B(8)	7	8	16	16	3	5	3	4	8	8
C(8)	12	4	7	9	7	5	28	0	6	0
D(7)	12	2	3	7	16	1	20	1	9	0
E(5)	6	4	4	4	9	3	3	3	7	3
F(4)	4	4	4	4	3	5	3	0	7	8
G(4)	5	3	6	2	7	3	2	1	8	6
H(4)	1	6	3	7	0	5	2	9	0	4
I(4)	4	4	4	1	7	8	5	4	0	1
J(4)	2	5	6	12	0	4	3	13	1	0
K(3)	2	4	2	4	3	8	1	2	0	1
L(3)	5	0	0	0	0	0	11	2	9	2

the particles suddenly reverses, and they stream northeastward until they leave the grid. This trajectory pattern shows a definite preference for the 0100-1200 MST release period when considered over all seasons. However, this seems to be due to its very strong occurrence during this period for the summer season. It is the most predominant pattern during the summer for the 0100-1200 MST release period with a 28 percent occurrence. In order of predominance for the 0100-1200 MST releases during the other seasons, it ranks third in the winter, fourth in the spring, and eighth in the fall. The only rankings this pattern has for the 1300-2400 MST release is fourth in the winter and eighth in the spring. This would indicate that this pattern is strongly related to the reversal of the winds due to the overall slope of the plain from the northeast to the southwest and the diurnal heating and cooling cycle.

The next pattern, designated type "D", also indicates a change in the flow pattern from northerly or northeasterly flow through southerly flow. The character of this pattern, however, indicates the change to be a gradual clockwise rotation of the wind instead of an abrupt reversal as in type C. The trajectory patterns that fall into this type give the first hint of a spatial difference in the winds over the area of concern. The winds near the bottom of the grid seem to be turning before the wind at the source. This type of pattern also showed a preference for the 0100 to 1200 MST release time except for the winter. Its most frequent occurrence was

during the spring when it ranked second behind type A. In almost every occurrence of this type the shift in the wind began between 0900 and 1100 MST.

The next type of trajectory pattern, denoted "E", is characterized by the particles streaming northeast for the enitre release period and leaving the top of the grid. The pattern indicates a sustained flow from a southwesterly direction. The relatively small percentage of the time that this type occurs through either release period is an indication that, although wind rose information indicates that the wind blows from this sector over 30 percent of the time, it does not do so in a sustained manner from the source to the top of the grid. The highest percentage of occurrence for this type is 9 percent for the spring, when it ranks third behind types A and D. This seems to contrast with the situation noted for type A, in which there was a very significant amount of sustained northerly flow. There is probably some bias introduced by the source being twice as far from the top of the grid as it is from the bottom. Also, since type C indicates the onset of the southerly wind is from 0900 to 1100 MST, a release period from 0900-2100 MST would probably show a higher occurrence of type E. One might also suspect that the contrast is due in part to the flow characteristics in the upper portion of the grid being generally more variable and complex than the southern part. This is indicated by some of the types yet to be discussed.

The next pattern shown, denoted type "F", is one that definitely indicates a spatial variation in the flow, because the trajectories are definitely curved and they show little variation with time. A single curved trajectory may be due either to the rotation of a straight flow pattern with time or to a curved flow pattern that remains stationary with time. This pattern of trajectories indicates flow from a westerly direction at the source and becoming southerly toward the top of the grid. The most predominant occurrence of this pattern is in the fall. For 0100-1200 MST release period, it occurred during 7 percent of the days and ranked seventh. For the 1300-2400 MST release period it occurred 8 percent of the days and ranked third. This is the first type to give an indication of the flow conforming to the curved depression in the topography. Releases from a source located in the lower right section of the grid would probably give a much clearer indication.

The next trajectory pattern, denoted "G", indicates light winds. Since none of the 12 particles released is carried off the grid, the winds were light and variable for at least 24 hours. The summer season shows the least

percentage of occurrence of this pattern. This is probably due to the predominance of the diurnal upvalley-downvalley flow. The other three seasons show from 6 to 7 percent occurrences for the 0100-1200 MST releases and 2 to 6 percent occurrences for the 1300-2400 MST releases. This indicates that a light and variable wind situation in the central portion of the grid has a stronger tendency to persist for 24 hours if it begins at 0100 than if it begins at 1300.

The trajectory pattern denoted type "H" is one of the most striking examples of spatial variation in the wind flow. This type is a manifestation of the circular eddy that was discussed in section 2.2.1. The occurrence of this type shows a definite bias toward the 1300-2400 MST release period, indicating that it is a late evening or early morning phenomenon. It occurs most frequently (9 percent) in the summer and ranks second behind type C, but the next highest occurrence (7 percent) of the phenomenon is in winter and ranks fifth. This trajectory pattern probably demonstrates most dramatically the contrast between the type of transport that might be deduced from a wind observation at the source and several observations over the entire area of interest.

The next three patterns, denoted "I", "J", and "K", show why type E does not occur more often than a wind rose would imply. Type I indicates southwesterly flow from the source becoming southerly about 90 km northeast of the source. The percentages shown indicate this condition to be most predominant in the spring. Type J indicates southwesterly flow throughout the release period but then a sudden reversal to northeasterly flow. The percentages shown indicate that it is most predominant during the 1300-2400 MST release and that it occurs most often during the summer and winter seasons. The relatively high percentage (13 percent) in the summer would be more than likely caused by the diurnal wind reversals, but the correspondingly high occurrence in winter probably would be due to frontal passages. Type K also indicates a southeasterly flow reversing to a northeasterly direction. The difference is that the direction change occurs earlier during the release period and it occurs as a gradual clockwise rotation. This type also shows a preference for the 1300-2400 MST release, but it occurs most frequently (8 percent) during the spring, in contrast to the summer and winter highs of type J.

The last type shown is designated "L" and also indicates a reversal in the flow pattern. The trajectory in this case indicates a light northerly flow changing to a stronger southerly flow in such a way that the particles are swept back across the grid in a line. This pattern shows a definite bias toward the 0100-1200 MST release period. It occurred only

during the summer (11 percent), in which it ranked third behind types C and D, and during the autumn (9 percent) in which it ranked third behind types A and D.

There are other types of patterns that are recognizable but occur with less frequency than those shown. Annually the 12 types shown account for about 74 percent of the flow patterns observed. Table 3 shows a breakdown by season and release period indicating how representative these patterns are.

The construction of the trajectories of particles released from the same location once an hour, and displaying them 12 at a time for a long period, provides information concerning the time changes and some of the spatial variation in the flow patterns in a more compact form than the wind field plots. The subjective typing of these trajectory patterns provides unique information about the possible influence of the area flow patterns on transport from a selected source location. The sample examined here is not large enough to be considered a true climatology, but the results obtained do indicate the types of transport patterns and their frequency of occurrence that might be expected during each of the four seasons. Trajectory plots of the kind used in this analysis depict the nature of this variation to the extent that one can distinguish between two types of wind reversals, as in types C and D. The distinction can be very important when one is concerned with the transport of an effluent over a short period of time. The wind field data may also be used to construct trajectories for determining transport statistics at various receptor locations for long period releases. An experiment of this type is described in one of the following sections.

2.2.3 Receptor Climatology

In a previous report of this series (NOAA Tech. Memo, ERL ARL-28, 1971), the initial work on trajectory frequencies to selected receptors was presented. That method transported hypothetical particles, released once each hour from a given source, in the NRTS interpolated wind fields. Counts of trajectories hitting optional targets of optional radius were made. This scheme shall be hereafter called the "significant target model." The trajectory hits are counted several ways to give total unique trajectory hits, total hits including repeated occurrences by the same trajectory, total number of periods in which trajectory hits were recorded, number of cases of discrete dwell periods where one or another of a series of particles is continuously over or passing over the target, and total dosage obtained by some mathematical

assumption combined with the count of total hits with repetition. Total dosage and number of periods are printed as one value and the other statistics are printed out in matrix form having as arguments, time of day of release, and elapsed time until hit; except the dwell times have total period of dwell as the latter argument. It was also shown that the number of recorded hits will vary with target radius in a linear manner for radii less than 7 or 8 miles. The slope of the line was very nearly 'two' where doubling the radius resulted in half again as many hits. This receptor climatology is very practical for studies in both nuclear reactor and industrial siting. In addition, this method is being used to study long-range diffusion by comparing dosages for periods of about a week. The details of these studies are in section 2.2.4.

The significant target model gives considerable detail at a given target; however, more often a siting study will want to know the climatology of trajectories as a pattern over an area of say one or two thousand square miles. A second model for the receptor climatology, called the "area pattern model," was developed to record trajectory hits in the squares of a grid over the geographical region of concern. Four statistical summaries were made and printed out in a matrix representing the grid. The summaries are number of unique trajectory hits, number of trajectory hits with repetition allowed, number of independent 12 hour time periods in which trajectories hit, and total dosage, which is again computed with some mathematical expression in combination with the trajectories-with-repetition count. The remaining discussions on receptor climatologies will be made using this area pattern model; however, the conclusions are equally applicable to the significant target model.

One of the first questions in using these models is how many wind recording stations are needed to get representativeness of the true climatology of transport? At the NRTS there are 21 wind stations from which the wind field is determined, while 33 were available for a study of the Los Angeles Basin. Receptor climatologies were computed with three assumptions on the transporting wind field to see the effect of having only one wind station available for a siting study. The first assumption is a wind transport field interpolated from all available wind records. It is assumed that this gives the true pattern, although it is recognized that vertical wind shear plays an important role in creating differences between the true trajectory climatology and the climatology resulting from the windfield assumption. The second assumption is that the wind everywhere is the same as the wind at one station, called the single-station analysis. The third assumption

assumes that once a particle is released it cannot change direction, which is a wind rose assumption. The wind rose assumption is used to determine whether significant information is gained by taking the single-station analysis when only one wind station is available. The wind rose pattern was smoothed by assuming an even distribution of trajectories over the arc covered by a direction ray. The single-station analysis of frequency of trajectory hits shows a very strong "spoking" of the isopleths. This is because the particles are being advected by winds of certain discrete directions, and the more cases of persistent wind direction at the base station, the more cases of particles streaming out along a straight line of the given direction. Before comparing the frequency of trajectory occurrence patterns of the single-station transport to the wind field and already smoothed wind rose transport assumptions, a smoothing of the single-station pattern was performed. The grid square of origin has a frequency of trajectory occurrence equal to the number of trajectories released, so is left unaltered. The four grid squares bounding the square of origin each intercept a number of the discrete direction rays from the source, and are therefore left unsmoothed since averaging over arcs of something like 90° is already accomplished. Border grid squares were smoothed by taking the average of the four bounding grid squares.

Figure 24 shows the frequency of trajectory occurrence in a grid square for the wind field, the smoothed wind rose, and the smoothed single-station transport assumptions for 2 years of NRTS data. The grid size is 4.29 km. Figure 24 shows the corresponding three panels for 1 month, September 1969, of Los Angeles data. The grid size here is 5 km. Both studies were based on 12 hour trajectories unless the trajectories left the grid in a shorter time. For the NRTS study the release point was PBF, marked with an "X," and single-station and wind rose analyses were taken from the SPERT wind station, less than 2 km away. For the Los Angeles study, the release point was "F," and the single-station and wind rose analyses were taken from the SOCO wind station, about 11 km northeast of the release point.

At the NRTS there is strong channeling of the winds into one of two directions, so there is significant similarity of pattern in all three panels of figure 24. Because of the rarity of west-northwest and east-southeast winds, the wind rose assumption resulted in a very narrow pattern. The single-station analysis allows wind shifts along the trajectories which means a greater spreading of the pattern. When compared with the wind field assumption the single wind station pattern is actually overspread. The probable reason for the overspreading is the effect of a shift in wind direction

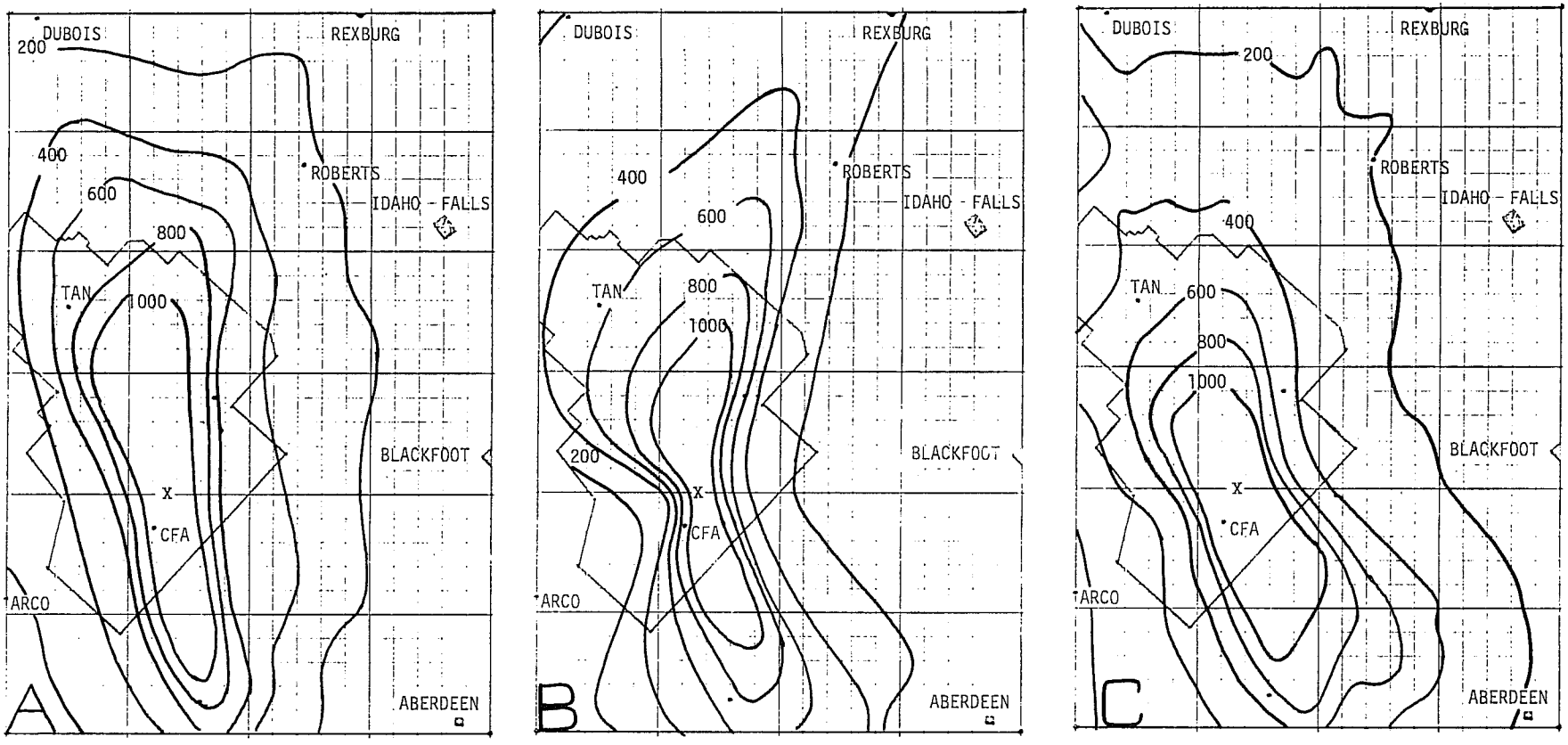

Figure 24. Isopleths of trajectory releases from PBF (marked as an 'X') for 2 years, once each hour (2280 trajectories released). A - wind field transport, B - wind rose transport, C - single-station wind field transport.

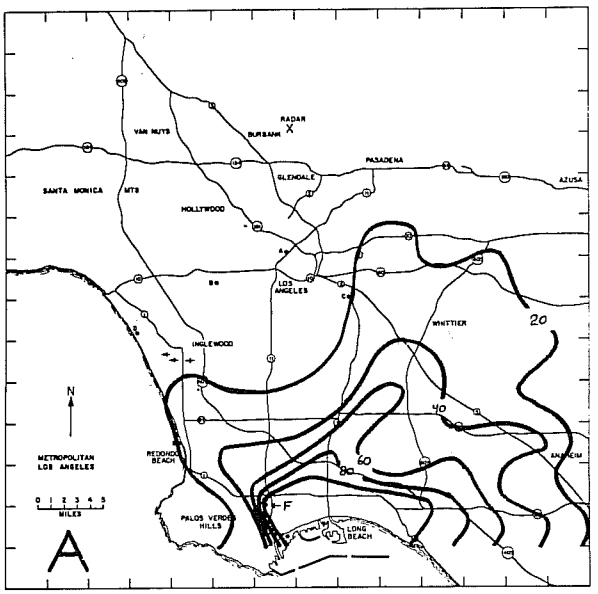
RADAR
BURBANK
VAN NUYS
PASADENA
GLENDALE
AZUSA
SANTA MONICA MTS
HOLLYWOOD
LOS ANGELES
WHITTIER
INGLEWOOD
20
40
60
80
N
METROPOLITAN LOS ANGELES
REDONDO BEACH
0 1 2 3 4 5 MILES
PALOS VERDES HILLS
LONG BEACH
F
A

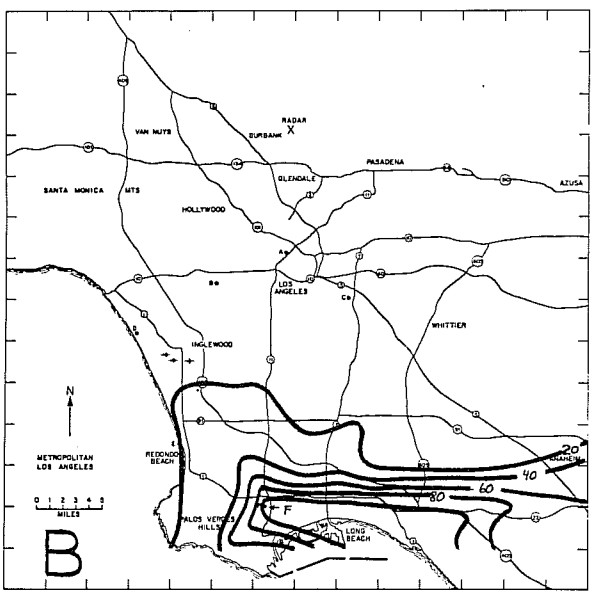
RADAR
BURBANK
VAN NUYS
PASADENA
GLENDALE
AZUSA
SANTA MONICA MTS
HOLLYWOOD
LOS ANGELES
WHITTIER
INGLEWOOD
20
40
60
80
N
METROPOLITAN LOS ANGELES
REDONDO BEACH
0 1 2 3 4 5 MILES
PALOS VERDES HILLS
LONG BEACH
F
B

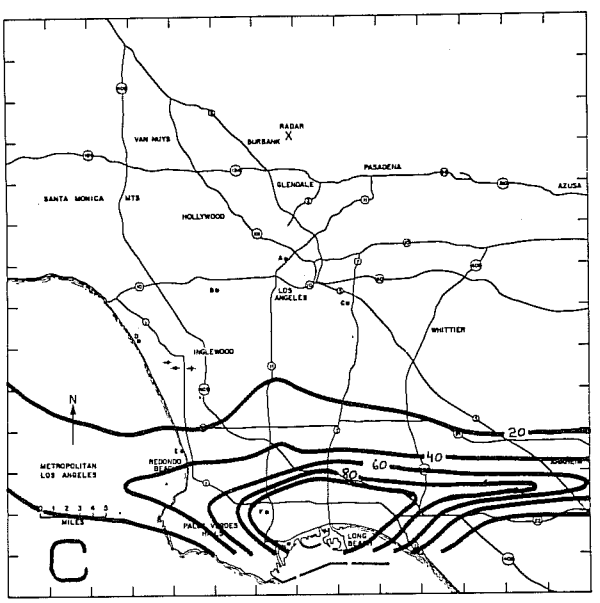

Figure 25. Same as figure 24, except 720 trajectories released for September 1969 at release point F at Los Angeles

using single-station analysis. If winds are from a fairly steady direction for several hours, the single-station analysis will show a stream of particles along the line of the wind direction. If the wind makes a shift of about 45 to 135 degrees the single-station analysis will result in a line source sweeping nearly broadside across the original line of flow. Numerous studies of trajectories in the 21 station wind field show this does happen, but more often the direction shift progresses across the field rather than occurring everywhere at once. These wind shifts result in some of the greatest case differences between single-station and wind field derived trajectories.

The ability to spread the frequency of trajectory occurrence pattern by the single-station assumption, as opposed to the wind rose assumption, was a distinct advantage in approximating the wind field results over the greater part of the Los Angeles Basin. A peculiar diurnal character of east to east-southeast winds at the SOCO wind station eliminated much of the spreading advantage by producing an unrealistic spoke in the frequency of occurrence pattern that crossed the Redondo Beach area. Both the single-station and wind rose results were significantly different from the wind field results, in that the latter showed significant transport to the Whittier area and the simpler transport assumptions showed very little transport to Whittier. The wind field analysis showed quite effectively the blocking by the Palos Verdes hills west of release point F, which the two simpler transport assumptions could not be expected to show.

Table 4 was derived to put some quantitative measure in the comparisons of results from the three transport assumptions. With the assumption that the wind field transport gives results very near to true, the table shows the linear correlations of wind rose and single-station frequency of trajectory occurrence pattern to the wind field pattern. Because the lateral diffusion of trajectories is approximately proportional to the square of the distance of travel, the grid squares were weighted by the square of their distance from the release point before entering the correlation. In the characteristic upvalley-downvalley flow at the NRTS the

Table 4. Correlations[1] of Wind Rose-to-Windfield and Single Station-to-Windfield With Square of Distance-From-Origin Weighting.

	NRTS	Los Angeles
Wind rose to windfield	0.848	0.521
Single station to windfield	0.786	0.612

[1]The grid square of origin is not included in the correlations

correlations are significant though the sample is too small to say the wind rose assumption gave significantly better results than single station. It appears the overspreading of the pattern by the single-station assumption was more serious in this experiment than was the underspreading by the wind rose assumption.

The more complicated wind patterns at Los Angeles resulted in rather poor correlations of the two simple transport assumptions to the wind field results. The spreading advantage of the single-station assumption did give better results in this study than did the wind rose results.

With a sample of only two studies, no conclusion can be drawn about the characteristic advantage of wind rose over single station or vice versa in studying the receptor climatology of an area. It appears that the more complex the local flow patterns the more a transport study using one wind station will depart from realism.

A second question of major importance is how long should the wind records be to be considered as representing a long term climatology? Table 5 gives the second moment correlation of the NRTS matrices of trajectory occurrences for two winters and two summers; all are shown in the four panels of figure 26. The two winters correlate to one another better than to either summer, and the two summers correlate to one another better than to either winter, which shows a reasonably stable seasonal pattern in the winds. All the correlations, however, are quite strong, indicating the NRTS is an area where the prevailing winds have comparatively little seasonal variation.

Figure 27 shows four panels of wind roses taken from 7 weeks of 1200 GMT data from each of four seasons at Portland, Oregon. The wind roses are to 16 points because the data were taken subjectively from the Daily Weather Map series of the National Weather Service. At Portland there is a very great seasonal difference in the prevailing winds. Summer patterns there will always be quite well correlated; however, winter patterns have a fairly strong variation according to the frequency of east winds down the Columbia Gorge.

Table 5. Correlations of Four Seasons to one Another. Data Weighted by Square of Distance From Origin. Grid Square of Origin not Included in the Correlations.

	Summer 1968	Winter 1969	Summer 1969	Winter 1970
Summer 1968	1.000	0.906	0.965	0.949
Winter 1969		1.000	0.893	0.935
Summer 1969			1.000	0.915
Winter 1970				1.000

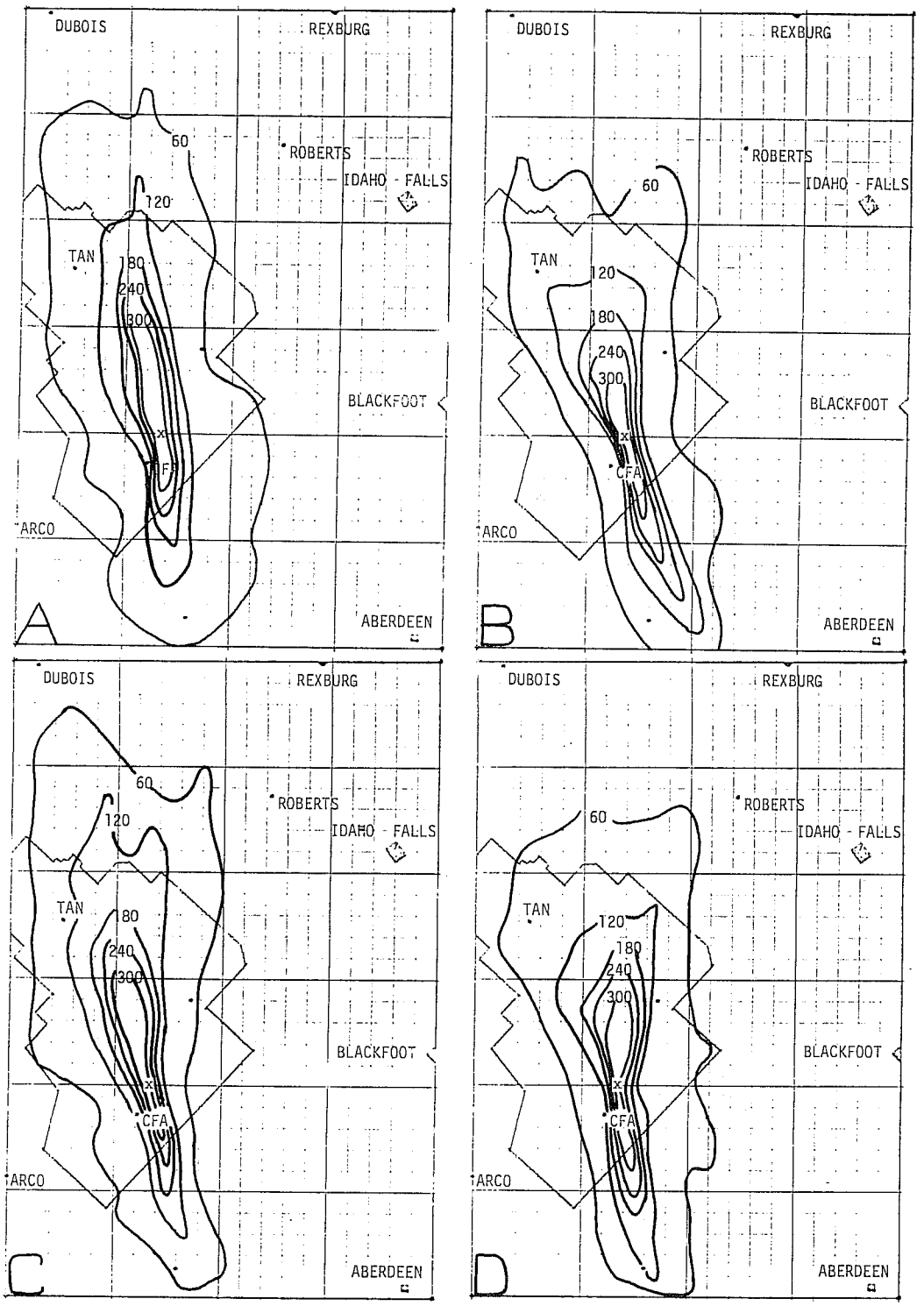

Figure 26. Isopleths of trajectory releases from PBF (marked as an 'X' for 2 years, once each hour. 2160 trajectories released on each of four seasons with transport by the wind field. A - summer 1968, B - winter 1969, C - summer 1969, D - winter 1970.

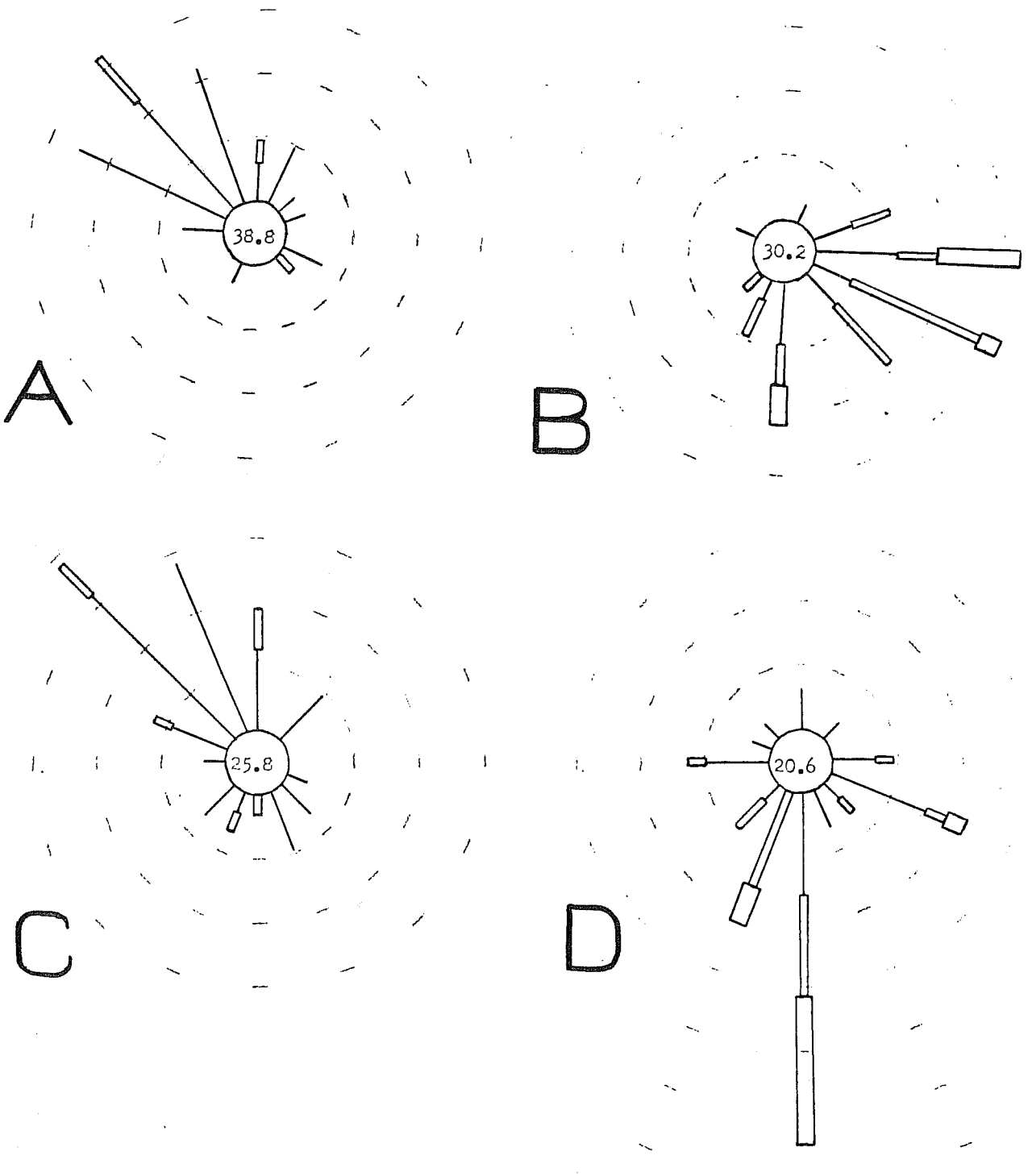

Figure 27. Sixteen point wind roses for 7 weeks of 1200 GMT data for four seasons at Portland, Oregon. A - summer 1969, B - winter 1970, C - summer 1970, D - winter 1971. Dashed circles for 5, 10, and 15 percent frequency, speed class 1-3, 4-7 mph, percent calm in center.

If wind records are not available for the immediate area of a prospective site, it would take at least 2 years to establish the prevailing patterns, because it would not be previously known whether the interseasonal and interannual variations were more like those of the NRTS or more like those of Portland.

Once wind records are available the receptor climatology models may be used for certain parts of the day and various periods of trajectory transport according to the application. One example from the Los Angeles data is given. The most typical time of the wind shift from nocturnal pattern to the heat-of-the-day pattern at the SOCO wind station was at 0800 PST. The two panels of figure 28 show the results of following 12 hour, wind-field-derived trajectories with 0800 and 2000 PST as the breaking points. Shorter trajectory periods would show a greater difference, since the nighttime trajectories largely head north to northwest; however, as the later nighttime trajectories reach the Inglewood and Redondo Beach area, the daytime sea breeze begins and carries these trajectories eastward. The daytime releases are carried rapidly north to east by the prevailing sea breezes.

The testing of computational logic between the two models, working of examples as given in this report, and establishing a standard output have progressed to where we feel the techniques for calculating them are operational.

2.2.4 Receptor Climatology vs. Weekly Environmental Monitoring

Trajectories were calculated using detailed tower-measured winds throughout the Upper Snake River Plain and the calculated numbers of weekly trajectory receptions at selected sites were tabulated. At these same selected sites, high volume air samplers provided weekly samples of particulate matter. The analyses of β-emitting particulate matter were converted to average weekly air concentrations of β emitters, e.g., μCi/cc. The object of the following comparisons was to evaluate the ability of the wind field calculated trajectories to determine the basic shapes of the weekly average air concentration distributions. A very limited number of sampler locations were operative; they were positioned mostly around NRTS reactor facilities as part of routine environmental surveillance. Receptors were at the locations shown in figure 29; the source was the 76-m stack at the Idaho Chemical Processing Plant (ICPP). Transporting winds for trajectory

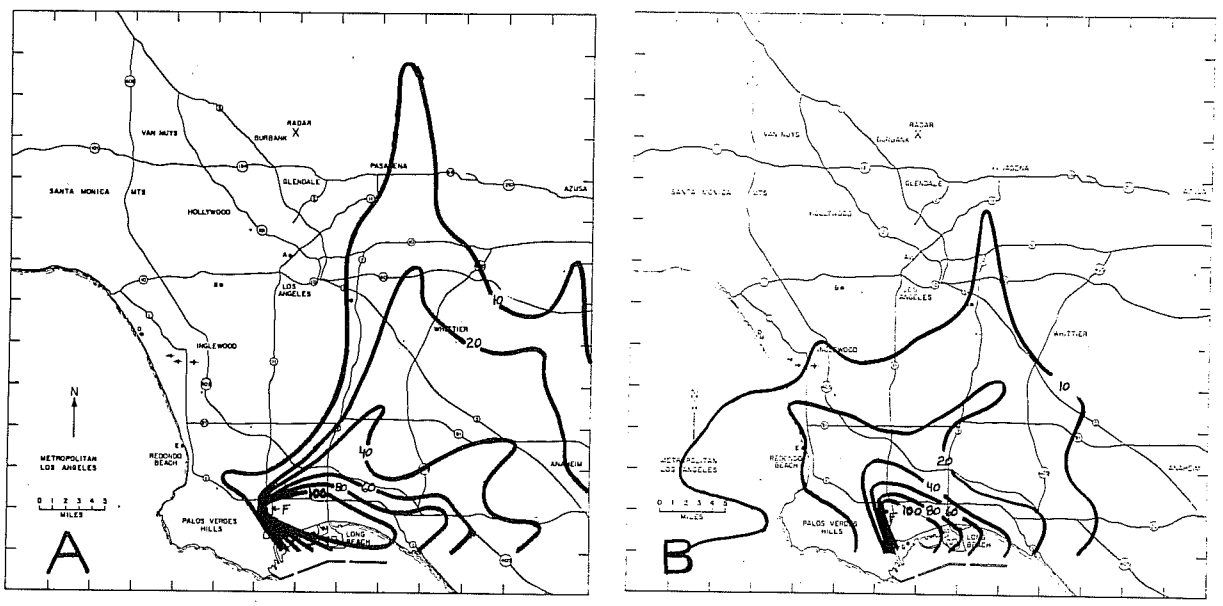

Figure 28. Isopleths of trajectory releases from PBF (marked as an 'X') for 2 years, once each hour. 360 trajectories released during 0900-2000 PST in A and 360 trajectories released during 2100-0800 PST in B.

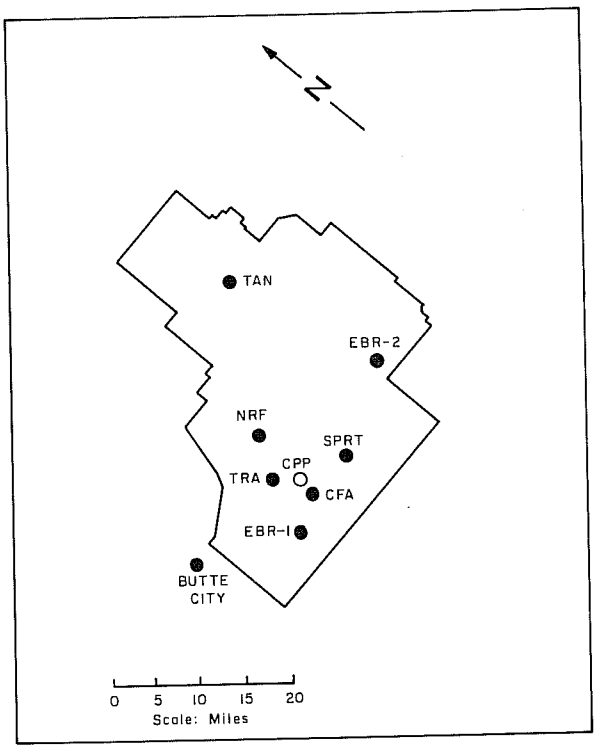

Figure 29. Source location and receptor sites.

calculations were determined from a network of stations within the Upper Snake River Plain (Wendell, 1970). These trajectories were calculated for 24 hours or until they left the computational grid, whichever was the shorter. Data from 4 successive weeks, August 22 through September 19, 1969, were evaluated in this study. Table 6 lists the values of concentration and the calculated numbers of trajectories affecting each receptor during each week.

Since the number of trajectories, by themselves, could in no way predict concentrations (multiplication by a constant would be simplest possible model) the data were put in a normalized form. Another benefit of normalization allowed data from different weeks and environmental conditions to be pooled. The concentrations were normalized by the concentration measured at the EBR-1 sampler site for this data set, where often the highest β concentration was measured each week. Another location could just as well have been used. For consistency the number of trajectory occurrences at the receptor points were also normalized by the number of trajectory occurrences at EBR-1. In figure 30 normalized ratios of concentration divided by normalized numbers of trajectory occurrences were plotted vs. straight line distance from the source. Half of the data points were within a factor of 2 of the line for a one-to-one relationship. While the data points scattered considerably at any given distance, the ordinate ratios tended to be proportional to distance to the -3/4 power.

To further probe the usefulness of this application of mesowind field calculated trajectories, a simple (and preliminary) prediction equation was developed to estimate weekly average air concentrations. The prediction equations used was

$$\chi(x,y) = (\bar{\chi}_0)(f(x,y)/f_0)(R(x,y)/R_0)^{-0.75}, \qquad (2)$$

Table 6. Weekly Values of Concentration[1] and Trajectory Occurrences

Location	Week No. 1		Week No. 2		Week No. 3		Week No. 4		Distance (km)
	$\bar{\chi}$	f	$\bar{\chi}$	f	$\bar{\chi}$	f	$\bar{\chi}$	f	
Butte City	0.3	75	5.1	20	10.1	85	16.0	23	26.4
EBR I	14.0	272	38.1	403	122.5	767	43.1	242	10.1
CFA	16.0	54	10.0	47	72.2	95	9.1	16	4.1
TRA	19.2	165	10.5	59	32.3	60	43.0	100	3.9
NRF	13.4	248	13.4	163	22.9	104	32.3	188	9.9
TAN	3.8	235	9.2	167	13.0	54	17.1	186	37.7
SPERT	--	20	1.0	16	26.1	32	9.7	23	9.1
EBR II	4.7	49	6.7	105	8.4	165	6.7	66	24.5

[1]All values of concentration are x 10^{-11} curies m^{-3}.

where

$\bar{\chi}$ = weekly average air concentration at location (x,y)

$\bar{\chi}_0$ = weekly average air concentration at the reference monitoring station

f(x,y) and f_0 = number of calculated trajectory occurrences at location (x,y) and the reference location, respectively

R(x,y) and R_0 = minimum distance from the source to location (x,y) and to the reference location, respectively.

The prediction equation is fundamentally a form of the conventional equation for long term average concentration in which the length of the averaging period is long compared with the time over which the mean wind is averaged (Slade, 1968). This conventional equation is normally used with wind rose data, the joint wind-speed and direction-frequency distribution. The normalized frequencies as would be used in the conventional equation, but instead of using point wind derived frequency statistics, the wind field derived frequencies of transport were derived for outlying receptor locations. Equation (2) was applied to the data in table 6

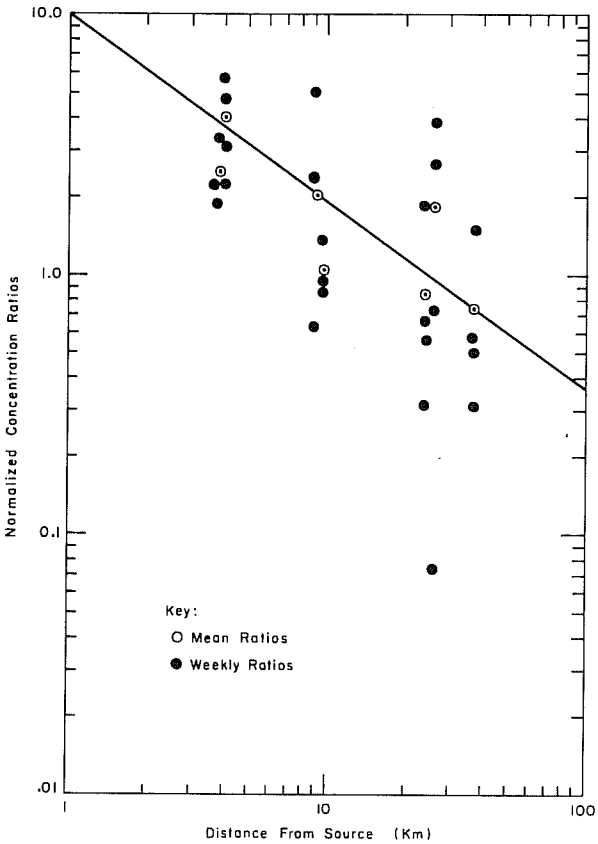

Figure 30. Normalized concentration ratios vs. minimum distance.

to test the technique. The results of the calculations are given in figure 31. There is a definite tendency for undercalculation for the cases examined in the pilot study. Two-thirds of the data points are calculated within a factor of 2 of the observed values, and three-fourths of the data points are within a factor of 3.

While the sample size is small, there seems to be preference for the largest undercalculations to occur for receptors located laterally from the source (lateral being defined as normal to a northeast-to-southwest line through the source). If so, the effect of terminating calculated trajectories at or before 24 hours after their beginning may be a contributing factor. Those receptors laterally displaced from the source (the northeast-to-southwest line through the source point parallels the principal axis of flow in the valley) would seem to be more frequently influenced by recirculated effluents than receptors northeast or southwest of the CPP stack. The initial success of this approach has indicated an enlarged examination of 2 to 3 years of data could be worthwhile.

2.2.5 Diagnostic Applications of Wind Speed and Component Spectra

The power spectrum of the horizontal wind speed presented by Van der Hoven (1957) shows a distribution of atmospheric kinetic energy covering a range of frequencies associated with synoptic scale through microscale motion. The major features of the mesoscale through the synoptic scale region of this spectrum have been recently substantiated in part by Oort and Taylor (1969) using data from several stations over a 10-year period and the very powerful Fast Fourier Transform (FFT) technique (Cooley and Tukey, 1965) for obtaining the

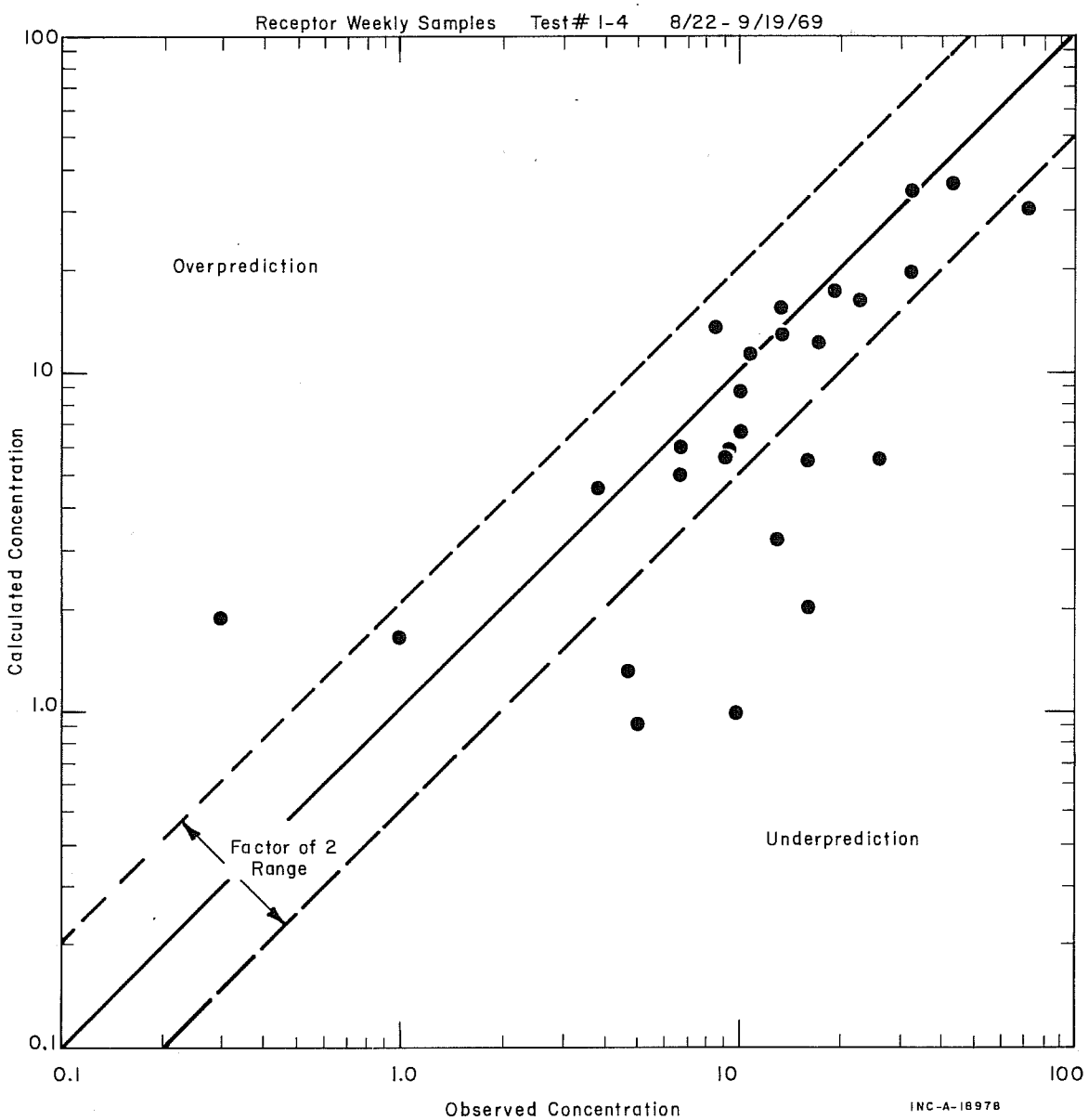

Figure 31. Results of calculations observed vs. calculated.

spectral estimates. This study showed some evidence of the spectral gap. Their results also agreed with those of Van der Hoven in showing that most of the variance of the wind speed is explained by the activity of traveling cyclones and anti-cyclones. Similar results have been reported by Vinnichenko (1970), although he also shows that the energy associated with the annual, synoptic, and mesoscale variations of the wind is much greater in the free atmosphere than near the surface.

Probably the most significant disagreement with Van der Hoven's spectrum was in the vicinity of the diurnal oscillation. He found no energy peak at a period near 24 hours, instead a minor peak appeared at a period of 12 hours. Oort and Taylor (1969) found a major peak at 24 hours and a minor, but noticeable, peak at 12 hours. They attributed this difference mainly to the 90 m height difference in the observations. Their data, observed at 10 m, were felt to be more representative of conditions within the surface layer and, therefore, more subject to diurnal oscillations. They did a very comprehensive analysis of the diurnal oscillation in the wind speed.

For comparison Oort and Taylor (1969) presented the separate energy spectra of the north-south (v) and the east-west (u) components of the wind for one of the stations. They concluded from this comparison that, at the station involved, there was a lack of an important diurnal cycle in the zonal and meridional wind components and interpreted this to mean that the diurnal cycle in the wind speed is not accompanied by a similar cycle in direction. They also indicated that the relative importance of an annual periodicity appearing in the u and v components of the wind showed a variation between locations. Another significant point of comparison was that the total variance in the component analysis was a factor of 3 greater than for the speed analysis over the same data sample. They attributed this to an additional degree of freedom added by the wind direction.

The difference between these two types of analyses is the concern here, as well as the insight into the nature of the oscillation which one can gain by their comparison. Also the merit of rotating the axes on which to determine horizontal wind component, in order to determine a principal axis of oscillation is investigated.

The total kinetic energy of the wind, by the nature of its definition, is independent of direction. Considering only the horizontal component of the wind, we can write

$$K_T = |V_H| = u^2 + v^2 \ , \qquad (3)$$

where u and v are orthogonal components of the velocity, generally taken to be positive to the east and north, respectively. For this analysis we shall omit the mass and factor of $\frac{1}{2}$ usually included in the definition of kinetic energy.

We may define the horizontal wind speed as

$$S_H = (u^2 + v^2)^{\frac{1}{2}} \tag{4}$$

which when squared, to obtain the kinetic energy, gives the same results as (3).

Several conventional meteorological wind sensing devices measure the wind in terms of horizontal speed (S_H) and direction (θ). Some, such as cup anemometers, measure speed only. Thus an analysis of the wind in terms of speed alone is not only convenient, but also sometimes all that is possible. Because the total kinetic energy is the same whether determined from the wind components or the speed, this fact would make this seem to be a minor problem. However, one doesn't have to make a very sophisticated analysis before the possibility of a serious discrepancy arises.

One of the simplest types of analyses that can be performed on a time series of wind data is computing the mean and the variance. When the variable being considered has units of velocity, the variance is taken to be proportional to the average kinetic energy of the deviations from the mean. The total kinetic energy can then be considered to be composed of the energy of the mean flow and the "eddy" flow,

$$V^2 = \bar{V}^2 + \overline{V'^2}, \tag{5}$$

where the bar represents a time mean over a specified interval, and the prime indicates a deviation from the mean. That there may be a significant difference in the mean and variance of the speed when compared with these same quantities for the components can be illustrated with a simple example. For simplicity, consider the horizontal velocity to be composed of a single component defined as

$$\left.\begin{aligned} v(t) &= A \sin t \\ u(t) &= 0 \end{aligned}\right\}, \tag{6}$$

where t is time and A is the amplitude. In the conventional sense, this would be a wind oscillating from north to south

and back again with a period of 2π and peak velocities of +A and -A. Wind measuring equipment that senses speed only would report only the speed fluctuation of the wind defined by (4) and can be written as

$$S(t) = A|\sin t| \quad . \qquad (7)$$

A comparison of the plots of (6) and (7) is shown in figure 32.

If we compute the kinetic energies of the mean flow (K_m) "eddy" flow (K_e) from these two series (integrating over 2π is sufficient), we obtain the values shown in table 7. Note that the total kinetic energy ($K_T = K_m + K_e$) is the same computed from either series. However, the division between the energy in the mean and "eddy" components is quite different, as one would expect from the comparison of the plots in figure 32. When direction is considered in this example there is no energy in the mean flow, it is all in the "eddy" flow. In the analysis of the speed data approximately 80 percent of this eddy energy appears as energy of the mean flow leaving only 20 percent as energy of the eddy flow.

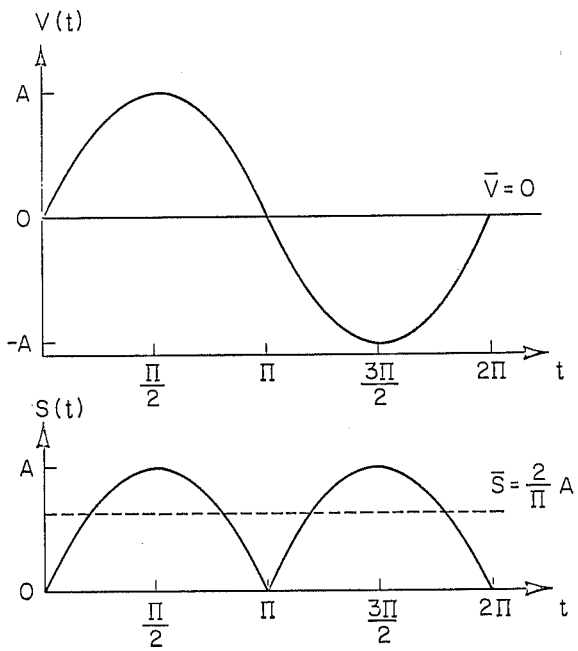

Figure 32. Comparison of velocity and speed for $V = A \sin t$.

If we now consider a Fourier analysis of the functions in the above example, we find that the transfer of eddy energy to mean energy is not the only problem. For the velocity variable (V(t)), we simply find all the energy appearing at the first harmonic with period 2π. For the speed variable (S(t)) we find no contribution to the variance at the first harmonic. The contribution to the variance from the rest of the harmonics is given by

$$K(n) = \begin{cases} 0 & n \text{ - odd} \\ \dfrac{8A^2}{\pi^2(1-n^2)^2} & \end{cases} , \qquad (8)$$

where n represents frequency in cycles per 2π. In evaluating (8) we find that about 95 percent of the variance of

Table 7. Comparison of Energy Values for Velocity and Speed Where V = A sin t, K_e = Eddy Energy, K_m = Energy of Mean Flow and K_T = Total Energy.

	Velocity V	Speed S
Mean	0	0.6366A
K_m	0	$0.4053A^2$
K_e	$0.5A^2$	$0.0947A^2$
K_T	$0.5A^2$	$0.5A^2$

S(t) is accounted for at n = 2. Thus we can summarize the effect of using the data from a speed sensor only to measure the wind, as depicted in (6), by saying that about 80 percent of the eddy energy appears in the mean flow and most of the remaining 20 percent appears at a frequency twice what it is for the velocity.

As drastic as these results seem to be, we need now to consider the wind of the example in terms of the real atmosphere. The wind defined by (6) would represent, in the atmosphere, a condition in which not only the speed is fluctuating (as defined in (8)) but also the direction is undergoing a cycle of complete reversals. This is the condition commonly observed on the shoreline of a large body of water or in a valley with a diurnal cycle in the direction and a semidiurnal cycle in the speed. A significant wind reversal cycle may also be noted with the passage of cyclones and anticyclones. The frequency of these cycles would depend, of course, on the size of the systems and the speed that they were translated. Thus one might expect the contributions to the total variance of these systems to appear over a broad band of frequencies.

Another phenomenon that can cause a strong variation in wind direction is one analagous to the cyclone-anticyclone example cited above but on a much smaller scale. This is one in which an eddy or group of eddies is imbedded in a translating flow that carries them past the wind sensor (Richter, 1964). If the eddies are strong relative to the translating flow, the direction can undergo as much as a complete reversal. However, if the eddies are relatively weak, the major effect will be a speed fluctuation. This can be visualized by superimposing a transporting velocity on to the oscillating velocity of (6) and writing

$$V(t) = A \sin t + B, \qquad (9)$$

where B is the magnitude of the transporting velocity. Clearly, if B is larger than A there will be no reversal of direction, and the mean and variance results for v(t) and S(t) will be the same. This is the condition that is generally sought for microscale turbulence analyses. It is the condition that usually prevails if there is more than just a light breeze blowing and the period of interest is less than a few hours. All of this brings us to the question of how one might interpret the differences and similarities in power spectra of horizontal wind speed and of the combined spectra of the components of the horizontal wind.

The first comparison of a wind speed spectrum and a wind component spectrum for a long data sample was by Oort and Taylor (1969). The comparison was made for a 10-year sample of hourly winds for Caribou, Maine. The diagram showing this comparison is shown in figure 33. In the original paper the wind speed spectrum was plotted in a separate diagram with a vertical scale magnification of about 2.8, which may have influenced the interpretation of the comparison.

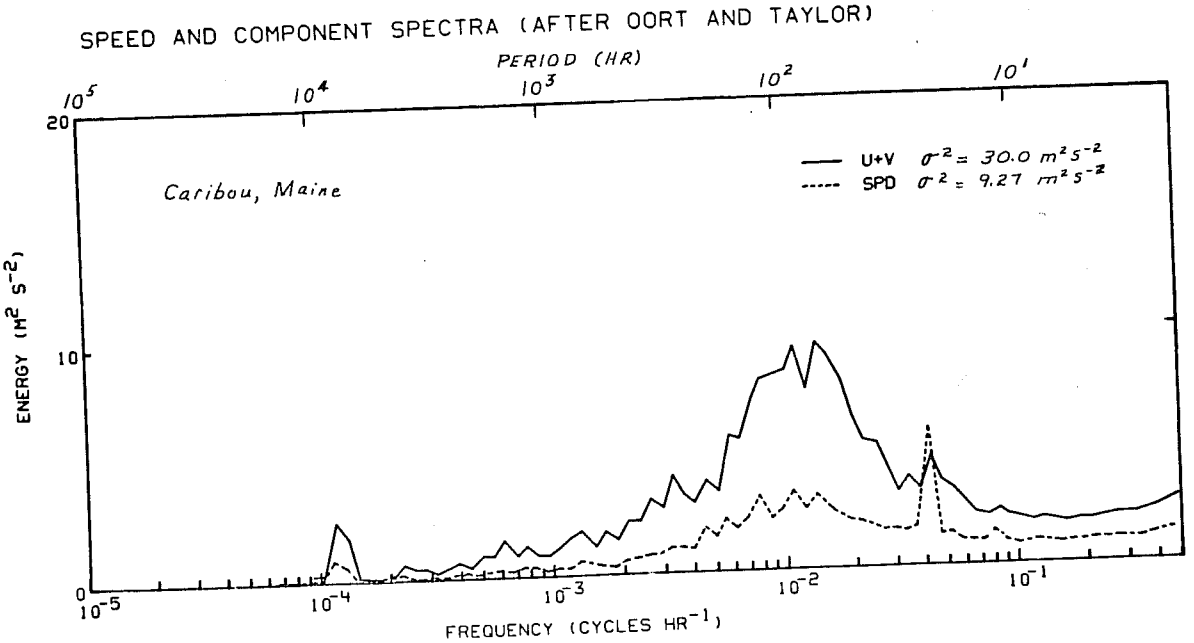

Figure 33. Comparison of wind speed and component spectra (after Oort and Taylor, 1969).

The increase of the total variance (by a factor of 3) for the component analysis was attributed to the addition of a new degree of freedom. From the considerations above, we may interpret the difference in total variance as a loss of energy of the oscillatory flow to the energy of the mean flow as obtained by using speed data only. The real case, considered here, shows a variance loss of 67 percent as compared with 80 percent for the simple example above. In examining the spectral curves in figure 33, we find that the frequency band hardest hit by this loss is for oscillations with periods of about 2 to 7 days. This is the band associated with the passage of cyclones and anticyclones. One might deduce from this result, without knowing the location of the station, that it lies in a location strongly affected by midlatitude storm systems.

Oort and Taylor (1969) pointed out, as the most interesting difference between the speed and component spectra, the lack of an important diurnal cycle in the zonal and meridional wind components. The interpretation was that the wind direction, near the surface, at the stations considered, is highly variable and does not follow a systematic diurnal cycle. When both spectra are plotted on the same graph, as in figure 33, we can see that the difference in the contributions to the variance near a frequency of one cycle day^{-1} is not nearly as impressive as the difference in the frequency band associated with the passing cyclones and anticyclones. The difference near the diurnal cycle is not so much a difference in magnitude (speed peak is 24 percent higher) but rather a difference in relative magnitude with respect to frequencies on either side of the diurnal cycle. When the frequency multiplication of the contributions to the variance is considered, the positive difference between the values of the speed spectra and the component spectra at a period of 24 hours is 16 percent of the negative difference between the spectral values at a period of 48 hours. In terms of the simple example of the previous section, the substantial energy deficit at a period of 48 hours in the speed spectra occurs because the velocity fluctuations involve direction very heavily at this period and enough of this deficit appears in the speed spectra at a period of 24 hours to cause it to exceed the component spectral value. The point to be made here is that rather than a lack of an important diurnal cycle in the zonal and meridional wind components, we find that, at this station, the contributions to the total variance by the synoptic scale disturbances are far more significant. The fact that these disturbances cause significant variation in the wind direction causes most of their contributions to be lost in the speed spectrum allowing the diurnal cycle to appear very prominent. Because the speed spectral

value at a period of 24 hours did not fall significantly from the component spectral value, we can deduce that the diurnal variation at this period is primarily one of wind speed and not direction.

We may show a contrast to this result by considering the energy spectra for both the wind speed and components for a station at the National Reactor Testing Station in southeastern Idaho. These two spectra have been computed for 8192 hours in 1969 for the 76-m level and are shown in figure 34. The spectral values have been multiplied by frequency in this diagram so that area under the curve will represent contributions to the variance. The speed spectra is quite similar to that for the Caribou, Maine, station, especially with regard to the predominant diurnal peak and the minor peak at 12 hours. The differences between the speed spectra and the

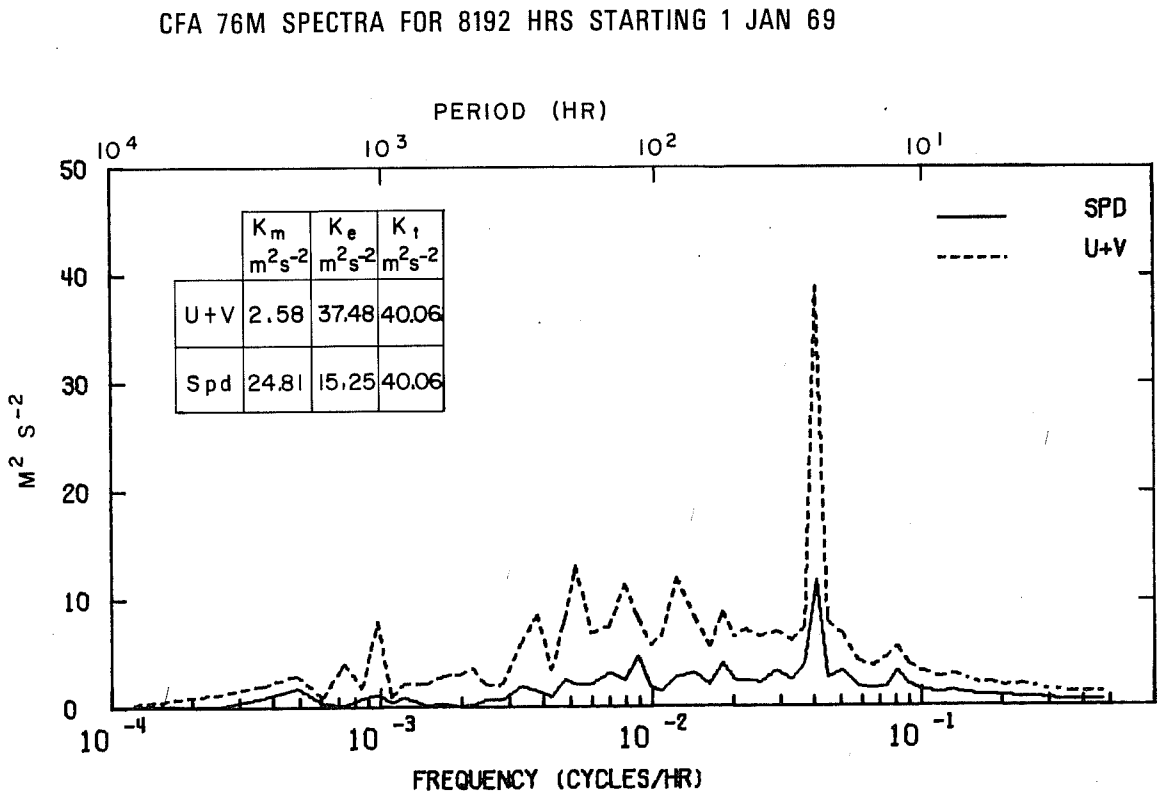

Figure 34. Comparison of wind speed and component spectra. The spectral estimates have been multiplied by frequency. K_e is equivalent to total variance, 76 meters.

component spectra are also quite similar except near the period of 24 hours. At this geographical location and height above the ground, the magnitude of the diurnal peak in the component spectrum is much greater than the height of the peak in the speed spectrum. There is about a 68 percent discrepancy at this frequency compared with the 80 percent for the sine wave example. This would indicate that the fluctuation in the velocity is primarily one of direction. This agrees with local observations of a diurnal wind reversal caused by topographic features in the surrounding area. The predominence of the diurnal peak at this location and level in the spectra varies from a maximum for the summer season to hardly noticeable for the winter season.

To indicate the dependence of the long range wind speed and component energy spectra with height, we show them in figure 35 for the same location and period at a level 6 m above

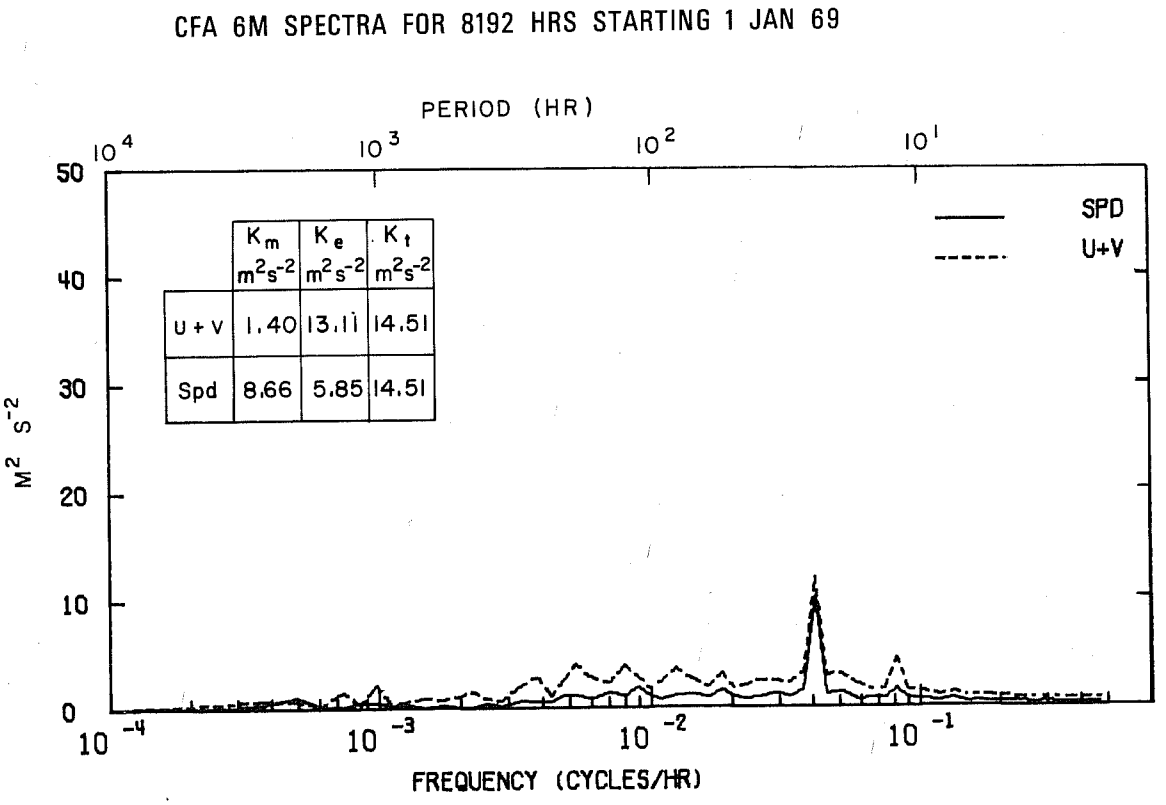

Figure 35. Comparison of wind speed and component spectra. The spectral estimates have been multiplied by frequency. K_e is equivalent to total variance, 6.1 meters.

the ground. We note, as would be expected, a much lower variance than for the 76-m level. It may also be noted that the distribution of the peaks are very similar, and that the energy discrepancy between spectra in the band of frequencies associated with synoptic scale disturbances is also similar. However, around the frequency of the diurnal cycle the simi-- larity ends. There is only a small difference between the speed and component spectra instead of the large difference observed at the 76-m level. This would indicate that the wind fluctuations at the 6-m level are primarily speed fluctuations instead of direction fluctuations. This is probably because the slope of the ground in the immediate vicinity of the tower is opposite the general slope of the terrain over the Upper Snake River Plain. This, plus surface frictional effects, would tend to oppose the general downslope winds near the surface. This effect would not be nearly as strong at 6 m during the afternoon, because the momentum of the general upslope flow would be transferred downward through convective mixing. The overall effect at 6 m is a relatively strong afternoon wind, but a very light nighttime wind with no significant reversal of direction as is observed at 76 m.

In the spectral plots of figures 33, 34, and 35 the horizontal velocity spectra are the direct sum of the spectra of the orthogonal components of the wind. The orientation of the axes from which the components are determined has no effect on the sum of the spectra of the components. Only under isotropic conditions, however, will it have no effect on the individual components. How then should we orient the axes? For long period data samples, the accepted convention is for the u and v components of the wind to be oriented in east-west and north-south directions, respectively. This orientation is well suited for the free atmosphere, because it facilitates the calculation of meridional transport. However, in the lower layers of the atmosphere, where surface effects are important, this orientation loses some of its usefulness.

The component spectra presented by Oort and Taylor (1969) showed only minor differences between the u and v spectra except at a period of 1 year. At this period there was somewhat more energy in the v (north-south) component than the u component. They pointed out that this difference in the component energy varied at different locations. The individual component spectra for the 76-m level of the NRTS tower are shown in figure 36 (the sum of these spectra is shown in figure 34). The conventional orientation of the coordinate axis has been used for the spectra shown in figure 36. Note that these spectra are quite similar, and without prior knowledge or further investigation one might be tempted to assume

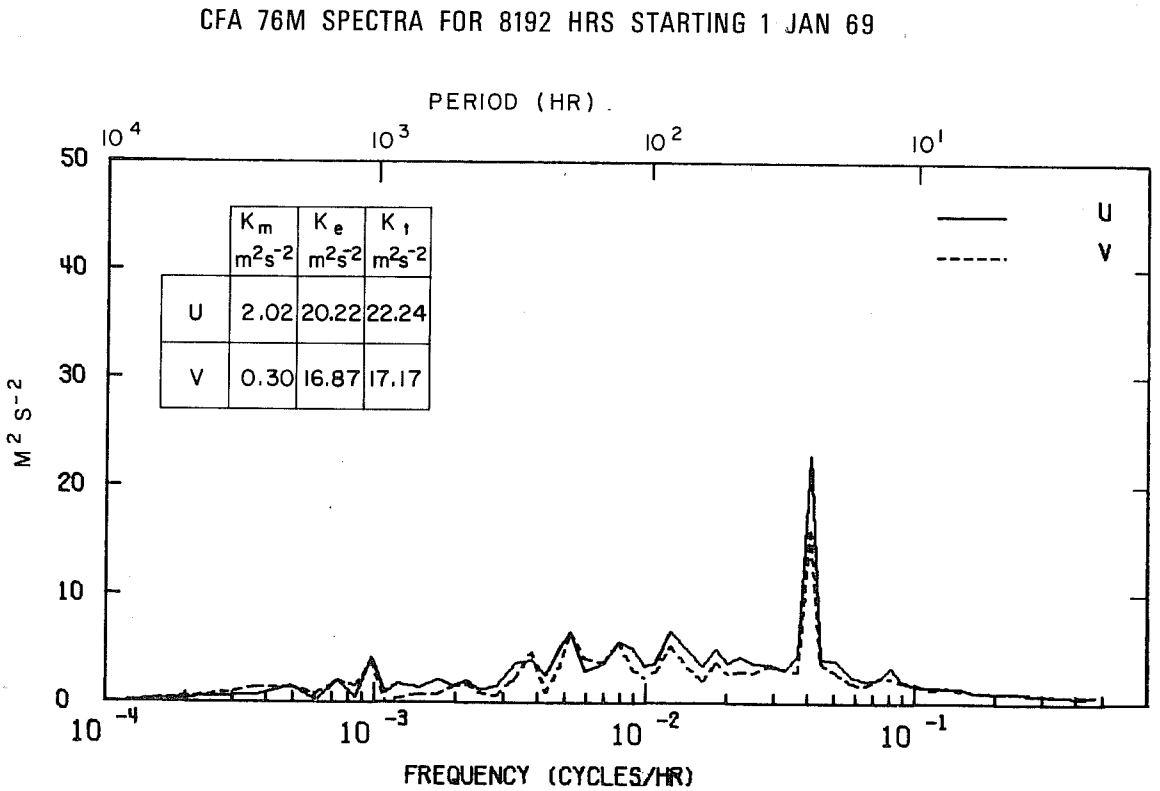

Figure 36. Comparison of component spectra for conventional orientation. In this diagram, v = north-south, u = east-west.

that near isotropic conditions exist at this level and geographic location. However, the power of the fast Fourier transform technique allows us to recompute, very inexpensively, the spectra for as many orientations of coordinate axes as we like.

In this case, rotation of the coordinate axes has some very drastic effects on the component spectra. The spectra for the same time period and level as shown in figure 36 are shown in figure 37, this time with a 49 degree clockwise rotation of the axes. For this orientation (v - northeast-southwest, u - southeast-northwest) the only portions of the spectra that are similar are for periods less than about 7 hours. For periods longer than 7 hours, a comparison of the spectra indicates that practically all the "eddy" energy is in the v component. In view of this result, we might consider 49 degrees to be the orientation of the principle axes of the turbulent energy for disturbances with periods greater than 7 hours at this level and geographical location.

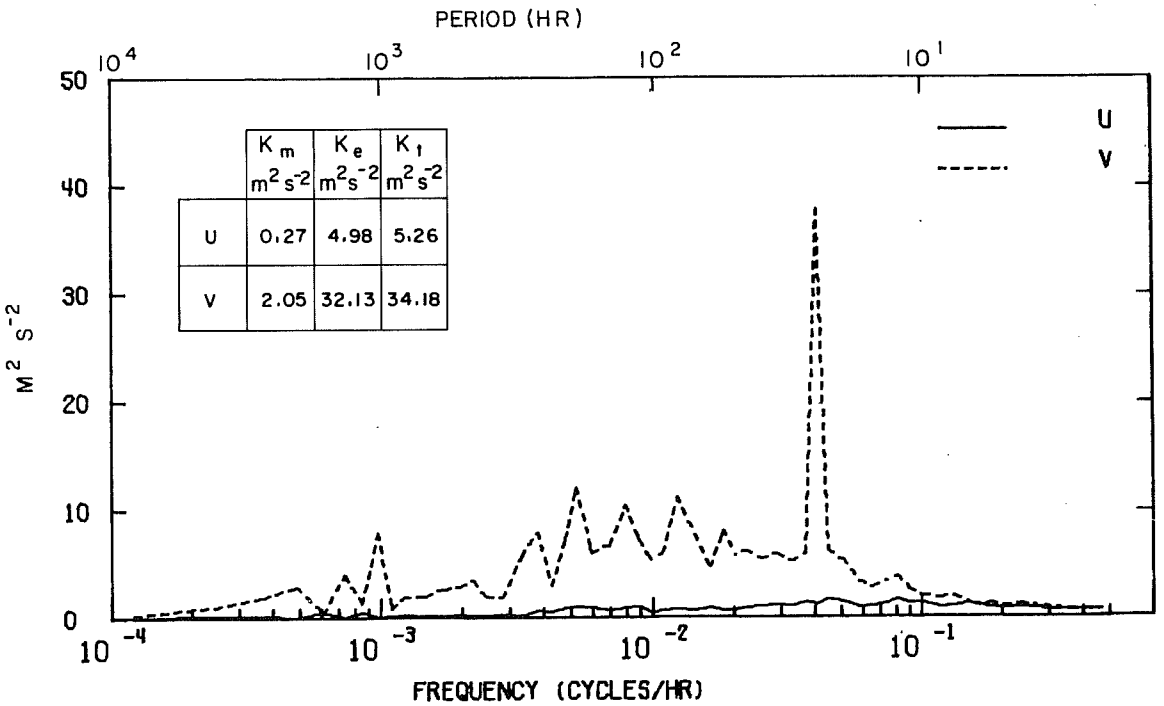

Figure 37. Comparison of component spectra for a 49 degree clockwise rotation from north. u = northeast-southwest, u = southeast-northwest.

As one might suspect this result is strongly influenced by the topography of the area, some of which has already been discussed. The gently sloping Upper Snake River Plain is approximately 60 miles wide and is bounded on both sides by mountains. These boundaries can be approximated by two parallel lines oriented at about 40 to 50 degrees (Dickson 1967; Wendell, 1970). These mountain barriers tend to channel the flow over the plain to a northeast-southwest orientation, as evidenced by the energy of the synoptic scale disturbances being almost entirely in the northeast-southwest component. The distribution of energy for the v component shows about 93 percent is "eddy" energy and 7 percent is energy of the mean flow (which is positive). This would indicate that for an effluent continuously released from location at 76 m, we could expect it to stream alternately northeast and southwest with the northeast direction being only slightly favored.

We can see from this example that observation of changes in the component spectra, as the orientation of the coordinate system is changed, can be used to advantage in determining the importance of various surface effects on the boundary layer motion. It is conceivable that in some locations, i.e., over the ocean, the component spectra would not change with a rotation of the axes. In other locations the spectra might not behave the same in different frequency bands under rotation. From spectra computed at other locations over the Upper Snake River Plain, it is apparent that there are differences in the behavior of the component spectra in the same geographical region. More extensive analyses of other stations and different years and seasons are being conducted.

The comparison of wind speed and component spectra for long periods for two different locations has shown that marked differences can occur. An energy analysis was performed on a simple one-dimensional model in which the wind was allowed to vary as a sine wave through both positive and negative values. This analysis showed that about 80 percent of the eddy energy of the velocity function appears in the energy of the mean speed, and almost all of the other 20 percent appears in the speed spectra at twice the frequency at which it appeared in the velocity spectra. This is not to say that the speed spectra is mathematically incorrect, because the speed spectra does accurately represent the frequencies at which the speed is varying. The difference is one of a physical nature and becomes important when the variation in the wind direction is through as much as 180 degrees. For sampling periods of more than a few hours, this situation can easily be realized; then an analyses of the speed alone does not realistically represent the division of the total energy into the "eddy" energy and energy of the mean flow, as well as the distribution of the eddy energy over the appropriate range of frequencies. This does not mean, however, that the computation of the speed spectra over long periods cannot serve a useful purpose.

The comparison of the speed spectra and the component spectra may be used to determine the nature of the velocity variation in the different frequency bands of the spectrum. If the energy in a given frequency band for the speed spectra is significantly less than the combined component spectra, then the velocity variation for this frequency band involves a direction reversal. If there is little difference between the two types of spectra for a particular frequency band, the velocity fluctuations in this band are then primarily speed fluctuations. The problem of about 20 percent of the difference between the spectra at a given frequency appearing in the speed spectra at twice this frequency does

not seem to seriously affect the comparison of the two spectra if it is kept in mind. With the type of information about the kinematics of the velocity variation provided by this spectral comparison, one has a better chance to find the physical caused involved.

This type of insight can also be provided by the component spectra through another comparison technique. This involves examining the changes in the individual component spectra as the coordinate axes, upon which the components are defined, are rotated. The results indicated that surface effects on boundary layer flow can cause conditions that are far from isotropic. A 49 degree clockwise rotation of the axes showed a fairly even division of energy between components change to a totally lopsided division of energy. This rotation can be done at any geographical location to determine the principal axes, if they exist, for the whole spectrum or any selected frequency band.

2.2.6 Methyl Iodide Mesoscale Dispersion Experiment

During the evaluations of a model developed to describe the spatial distribution of time integrated concentrations for effluents released from a continuous point source, a number of questions arose about techniques used in the model. One question concerned the accuracy of the transporting windfield; another question dealt with the validity of extrapolating rates of diffusion outward to 50 to 100 km downstream from the source. The following paragraphs describe observations of effluent transport to nearly 50 km downwind and comparisons of observed concentrations with the expected NRTS diffusion climatology concentrations. The NRTS diffusion climatology was developed principally from measurements of uranine dye concentrations within the first 3.2 km downwind of the release point. Extrapolation of this climatology to long distances, with Fickian diffusion beyond 20 km downwind, was used to obtain expected axial concentrations of uranine dye.

A field experiment on March 3, 1971, consisted of a 64-min release of methyl iodide from the 250-ft stack at the Idaho Chemical Processing Plant. The general weather conditions were a strong westerly flow above the mountain tops ahead of shallow, but intense, upper level disturbances centered over Vancouver Island. A northeast-southwest oriented Pacific cold front was moving across southern Idaho during the day. The ground was snow covered except for occasional windswept outcroppings of lava rock. A high thin broken

cloud layer existed at midday. By 1700 MST middle level cloudiness had increased from the southwest and snow showers developed and engulfed the mountains to the west and north of the NRTS. Temperature profile measurements from the 61-m Grid III tower showed lapse conditions with a range of 0.5 to 1.0°F per 100 ft during the test. The mean wind at the tower top was 228 degrees at 10.3 m sec^{-1}. Air temperatures were near 35°F.

To examine the atmospheric transport, we compared the observed mean plume centerline, tetroon trajectories, and "surface" trajectories calculated from the NRTS network of tower mounted wind sensors (Wendell, 1970). Figure 38 compares the tetroon trajectory at the beginning of the methyl iodide release (lower case letters) with the "surface" trajectory (upper case letters). The letter "a" denotes the tetroon position at 1 hour following release, "b" denotes 2 hours, etc. Figure 39 compares the trajectories initiated about two-thirds of the way through the effluent release (about 40 min later). In both cases the trajectory tracks are very close to one another. The times when the hypothetical particle (carried by the surface winds) and the tetroon

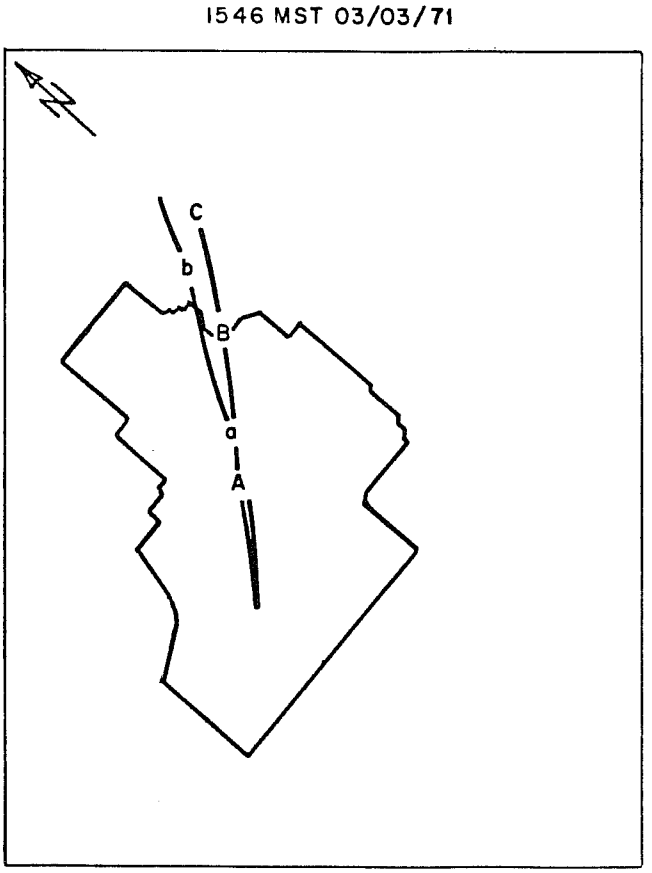

Figure 38. Comparisons of tetroon trajectories at beginning of methyl iodide release. Lower case letters and surface wind field calculated trajectories (upper case) letter A, B, C, etc., denote particle positions at successive 1-hour intervals following release.

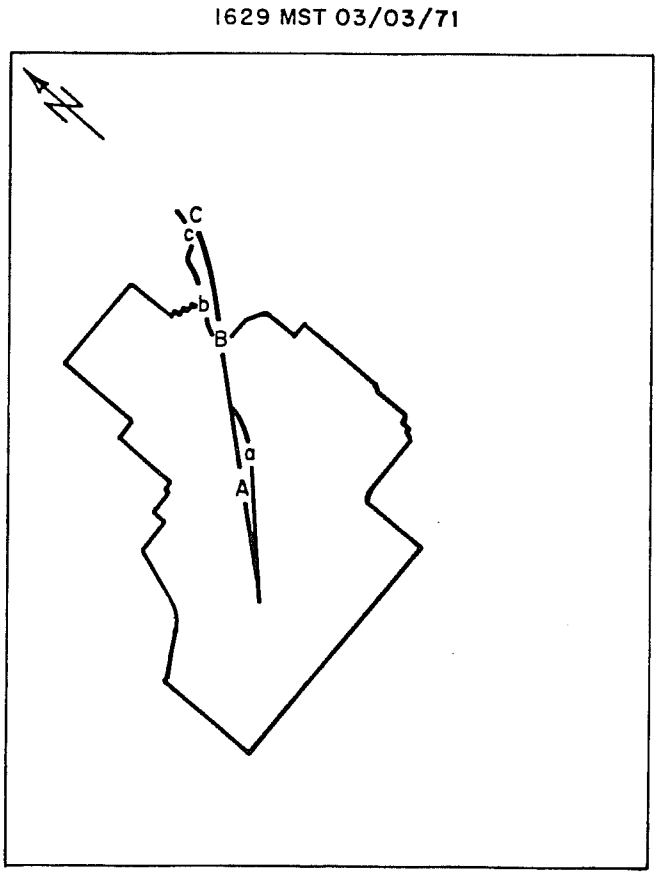

Figure 39. Comparisons of tetroon trajectories at beginning of methyl iodide release. Lower case letters and surface wind field calculated trajectories (upper case) letter A, B, C, etc., denote particle positions at successive 40-min intervals following release.

past over given points were different. This difference is well explained by the vertical speed shear (the direction shear was negligible). A mobile pilot balloon (pibal) wind unit moved upvalley with the approximate middle of the plume. The pibal winds compared very well with the directions and speeds of the tetroon movements as they moved through the areas of the pibal observations. The surface trajectories, when adjusted for the increase in wind speed at the tetroon flight level, approached coincidence in time with the tetroon trajectories. Most of the flight time the tetroons were 200 to 300 m above ground and moved at 13 and 16 m sec^{-1}. At 50 to 58 km downwind, the tetroons descended to within 30 to 60 m of the ground and nearly stagnated. The tetroons were visually sighted by the mobile pilot balloon observer. A pibal near points "c" and "C" in figure 39 confirmed very light winds in the atmospheric layer within 200 to 400 m above the ground.

Three air concentration sampling arcs were established at 3.9, 18.5, and 47.5 km downwind. Since these sampling areas were at remote sites high volume air samplers were positioned with a portable electric generator at each sampling location. Generator failures at 3.9 km eliminated data from that arc. Eight samplers were positioned on the 18.5 km arc and seven samplers were at 47.5 km. The sampling arcs are schematically shown in figure 40. Each high volume air sampler consisted of a Gelman E filter and a MSP46727 iodine activated charcoal cartridge. The collection efficiency of the sampling packet was near 0.70 for methyl iodide gas. The measured concentrations were plotted vs. angular bearing from the source in figure 41. The positions of trajectory crossings were shown by a short horizontal line near the peak arc sampled concentrations. The agreement at 18.5 km is excellent; at 47.5 km the agreement is good. The difference in angular bearing of the peak sampled concentration at 47.5 km and the envelope of trajectory crossings is not significant. The difference in position, approximately 2 km lateral displacement, is small compared with the spacing of samplers. Trajectory angular bearings as they crossed the 57.5 km arc are resolved to ±1 to ±5 degrees, for the tetroons and measured tower winds. Again, the difference in positioning is of the same order as the directional resolution of the trajectories.

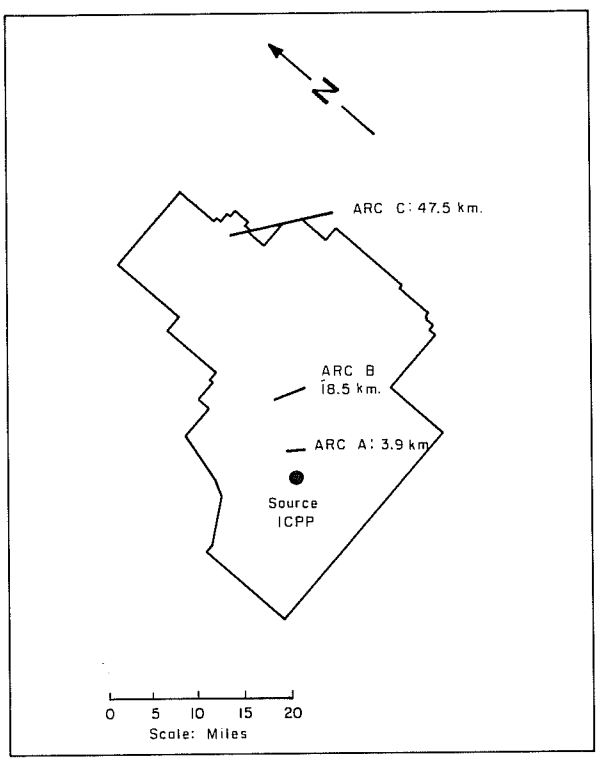

Figure 40. Location of sampling arcs and 250-ft source point stack.

The stability category during the stack gas release was class D, determined both by subjective considerations of insolation, wind speed, and cloud cover, and by bivane fluctuation statistics measured on the 200-ft Grid III tower approximately 2 km north of the source. Table 8 compares the expected axial

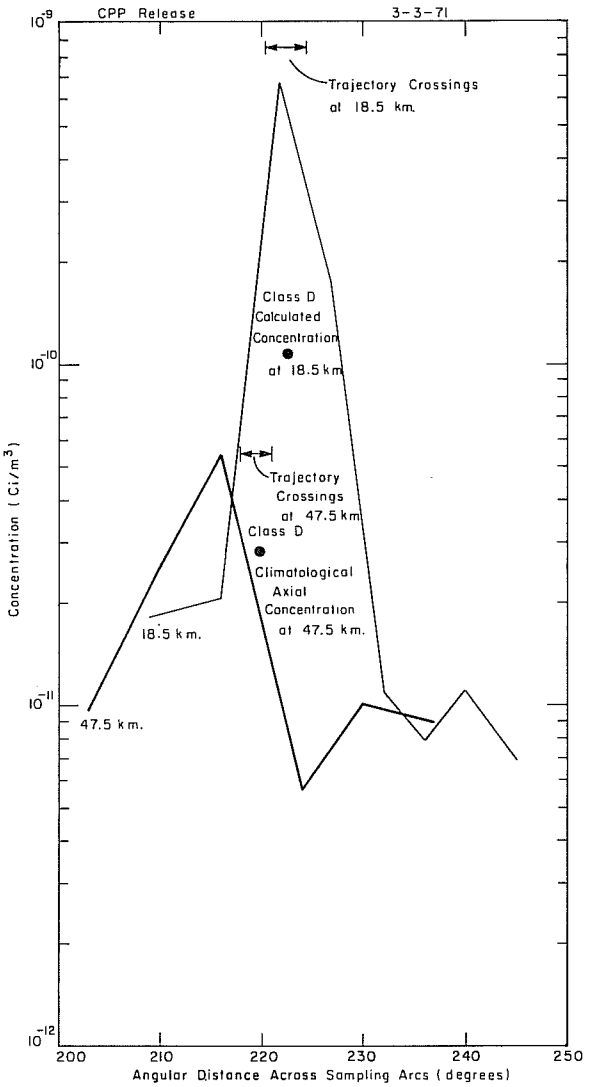

Figure 41. Measured concentrations vs. angular bearing from source.

concentrations for class D stability with the peak measured concentrations. The two ratios of observed-to-expected uranine dye axial concentrations in table 8 are of the same order or larger than ratios reported by Niemeyer and McCormick (1967). They reported ratios of sulfur hexafluoride (SF_6) to fluorescent particles (FP) for a range of 35 to 115 km downwind. Their mean ratios ranged from 1.0 to 4.9, with an average ratio of 3.3. Their conclusions were that the high average ratio may have been either due to FP fallout (plume depletion) or, since the ratios were not systematic with distance, due to possible sampling errors.

The concentrations sampled at the 47.5 km arc during this experiment seemed too small, and the concentration ratio should have been more comparable with the ratio determined for 18.5 km. The low axial value of concentration at 47.5 km (and other arc values also) apparently resulted from nearly two-thirds of the plume passing aloft over the sampling arc. The surface winds observed at the northwest end of the arc were light northerly or calm during what would have been the first 45 min of plume passage over the arc. Southwesterly winds occurred during the remainder of the plume passage, suggesting a final breakdown and elimination of the stagnant pocket of air that had covered at least some of the sampling arc at 47.5 km. The ratio of methyl iodide to expected uranine dye concentration at 18.5 km compared within reason to measured ratios of 4.5 within the first 800 m downwind of a paired tracer ground level release (Start, 1970).

Table 8. Measured vs. Expected Climatological Axial Concentrations

Distance (km)	Class D	Observed	Ratio
18.5	1.07×10^{-10}	6.75×10^{-10}	6.3
47.5	2.99×10^{-11}	5.4×10^{-11}	1.8

The following points may be summarized from the March 3 test. For the strong-wind, near-neutral atmospheric conditions examined by this case, the tetroon trajectories and the surface wind field calculated trajectories both accurately predicted the locations of the peak sampled air concentrations of methyl iodide. The measured concentrations of methyl iodide (in inert gas) exceeded the expected concentrations of uranine dye (FP) at 18.5 and 47.5 km downwind. The underprediction of methyl iodide agreed, in general, with previous comparisons between uranine dye and methyl iodide within the first 0.8 km and qualitatively with the observations of Neimeyer and McCormick (1967). This test has demonstrated that the technique is practical. Additional field measurements performed under other stability categories could be of value. The measurements at 47.5 km should be repeated during conditions that do not result in the plume passing aloft over the sampling arc.

2.3 Automated Processing and Graphics for the Large Data Base 1969 Los Angeles Study

The Los Angeles tetroon data were recorded directly to seven track (BCD) magnetic tape using an incremental type tape deck. One tape often contained several tetroon runs with the runs separated by an end-of-file mark on the tape. Each tape was processed through a screening program to determine the length of each physical record, number of records in each run, parity errors, and proper placement of end-of-file marks. Adjustments in final processing could be made for runs with parity errors, since the record where the error occurred was known. Also, runs with no end-of-file mark usually produced an inconsistent word count for the last record of flight.

The original data recorded in BCD were read and translated for time, range, elevation, and azimuth data as recorded by the radar at sampling rates of a few seconds for the first 44 flights and 1 sec samples for the remaining 61 flights. The instantaneous readings were rewritten on nine track magnetic tape in binary form at 1600 BPI for any further reference to the original data. The data were then averaged to give a range, azimuth, and elevation for each minute of flight by averaging six data points for the 10 sec data and 60 points for the 1 sec data. From these averaged 1 min data, the x, y, and z coordinates of the tetroon at each 1 min interval were computed with earth curvature corrections applied to the tetroon height (z). From the x, y, and z coordinates and the u, v, and w components, wind direction and speed at each 1 min interval were computed. Means and variance for the length of the flight were calculated for these parameters. Terrain heights on a rectangular grid of the Los Angeles basin, with grid spacing of $\frac{1}{2}$ km, were interpolated between grid points for each 1 min interval using the x, y coordinates of the tetroon. Terrain height and the height of the tetroon above the terrain were listed each minute. Flight statistics for each individual flight were listed on microfilm with the flight summary data following each flight.

The tetroon trajectory for each flight was plotted on 35-mm microfilm. Coordinates of major freeways and coastlines were extracted from a base map of the Los Angeles area. These x and y coordinates were entered on punch cards at any significant change of course in the freeway or coastline. A key word was punched at the beginning to turn the light in the CRT on, and at the end to turn the light off, of the freeways and coastline. Names of towns were drawn using standard hardware routines. The path of the tetroon was then traced onto the map with ascending alphabetic letters at each half-hour location of the tetroon after launch. To complement the x, y plots tetroon height vs. time microfilm plots were drawn. The terrain height under the tetroon was hashed vertical between sea level and the terrain height trace at each 2 min interval for contrast. The terrain data, originally on punch cards, were read to the "on line" disk pack storage for immediate access.

Hourly wind data from 20 Los Angeles county air pollution control district stations were obtained for September 1 through October 2, 1969. In addition, wind data were available from 13 aviation weather reporting stations in the Los Angeles area. These hourly wind data were converted to 36 point directions (Los Angeles County Air Pollution Control District data only) and sorted and merged to disk storage. Thus any hour within the period could be immediately accessed

for all 33 stations. By using the wind field program originally written for the mesonetwork stations in the Snake River Plains of southeastern Idaho, we computed the hourly u and v components for each station. These components were interpolated to a 69-by-60 km grid with 3-km grid point spacing. This technique has been described (Wendell, 1970).

Modifications were made to existing hypothetical trajectory programs for comparison of the tetroon trajectories to surface derived trajectories using surface wind data from the 60-by-69 km grid. Surface trajectories originated at the launch site at launch time and at the actual tetroon's location at each hour thereafter. The hypotehtical trajectories were determined from hourly wind fields, previously described, by 5 min time steps using interpolated u and v components from the four nearest grid points to calculate the displacement of trajectory for that time step. Linear time interpolation was used between consecutive hourly averaged wind fields.

Computer plots were made that compared the tetroon trajectory to each hourly surface derived trajectory. The tetroon trajectory was labeled with upper case letters to represent the tetroon location after each hour. The surface trajectories were labeled with lower case letters. To avoid clutter a new map was drawn for each hour of flight showing the entire tetroon trajectory and the surface trajectory released at that hour.

For the animated tetroon movies the tetroon location was indicated by an inverted triangle. Twelve 16-mm film frames represented 5 min of actual flight time of the tetroon, or triangle, in the x, y plane. Height of the tetroon above sea level was indicated by a vertical scale drawn to the right of the triangle. Terrain height was illustrated with a rectangular block under the triangle, where the top of the block indicated the terrain height. As the triangle traces the tetroon's path across the map and shows lateral movement, the scale is moved up or down to give the tetroon's height at the bottom point of the triangle. The tetroon flights selected for movie production were processed through an editing program that printed a still plot at every 10 min interval of flight. From these plots any outstanding features concerning the flight could be seen.

Methods and software for these routines are operational and applicable to any location given appropriate input data.

3. REFERENCES

Briggs, G. A., (1969), Plume rise, nuclear safety information center, Div. of Tech. Info, USAEC. Oak Ridge, Tenn.

Cooley, J. W., and J. W. Tukey (1965), An algorithm for the machine calculation of complex fourier series, *Math. Comp., 19*, No. 90, 297-301.

Crawford, T. V., (1966), A computer program for calculating the atmospheric dispersion of large clouds, UCRL-50179, Lawrence Radiation Lab., Livermore, Calif.

Dickson, C. R. (Ed.), (1967), Meteorology for the loss-of-fluid-test reactor, Progress Report, IDO-12059, U.S. Atomic Energy Commission, Idaho Falls, Idaho.

Dumbauld, R. K., (1962), Meteorological tracer technique for atmospheric diffusion studies, J. Appl. Meteor., *1*, 437-443.

ESSA Tech. Memo., Atmospheric transport and diffusion in the planetary boundary layer, Air Resources Laboratories Semiannual Research Program Review, July-December 1967, USAEC, ERLTM-ARL 20, 62 pp.

Hanna, S. R., (1968), A method of estimating vertical eddy transport in the planetary boundary layer using characteristics of the vertical velocity spectra, J. Atmos. Sci., *25*, 1026-1033.

Herbert, G. A., (1970), An interim evaluation of the airborne turbulence measurement system used in the Pendleton Project, ERLTM-ARL 21, pp. 16.

Herbert, G. A., and W. H. Hass, (1971), The Pendleton Project — a study in the atmospheric effects on weak shock waves traversing long ray paths, ERLTM-ARL 34, prepared for DOT under agreement DOT-FA69WAI-157.

MacCready, P. B., Jr., R. E. Williamson, S. Berman, and A. Webster (1965), Operational applications of a universal turbulence measuring system, NASA CR-62025, prepared under NASA/FRC Contract NAS 4-784. (AFB, Edwards, Calif.).

MacCready, P. B., Jr., (1966), Operational applications of a universal turbulence measuring system, AMS/AIAA paper 66-364, presented at the Conference on Aerospace Meteorology, Los Angeles, Calif.

Niemeyer, L. E., and R. A. McCormick (1967), Some results of multiple-tracer diffusion experiments at Cincinnati, Air Resources Field Research Office, ESSA, Cincinnati, Ohio, 86 pp.

NOAA Tech. Memo., Atmospheric transport and diffusion in the planetary boundary layer, Air Resources Laboratories Semiannual Research Program Review, January-July 1970, USAEC, ERLTM-ARL 28, 42 pp.

Oort, A. H., and A. Taylor (1969), On the kinetic energy spectrum near the ground, Mon. Wea. Rev., *97*, 632-636.

Readings, C. J., and D. R. Rayment (1969), The high-frequency fluctuations of the wind in the first kilometer of the atmosphere, Radio Science *4*, 1127.

Richter, A. P., (1964), A note on horizontal eddies of the mesoscale, J. Appl. Meteor., *3*, 339-342.

Rider, L. J., and M. Armandariz, (1966), A comparison of tower and pibal wind measurements, J. Appl. Meteor., *5*, 43-48.

Slade, D. H., (Ed.), (1968), Meteorology and atomic energy, TID-24190, (Clearinghouse for Federal Scientific and Technical Information, U.S. Dept., of Comm., Springfield, Va).

Start, G. E., (1970), Comparative diffusion and deposition of uranine dye, molecular iodine gas, and methyl iodide gas, Proceedings of Fifth Annual Health Physics Society, Mid-year Tropical Symposium on Health Physics Aspects of Nuclear Facility Siting, Health Physics Society, 463-473.

Van der Hoven, I., (1957), Power spectrum of horizontal wind speed in the frequency range from 0.0007 to 900 cycles per hour, J. Meteor., *14*, 160-164.

Vinnichenko, N. K., (1970), The kinetic energy spectrum in the free atmosphere — 1 second to 5 years, Tellus, *22*, 158-165.

Volkov, Y. A., V. P. Kulcharets and L. R. Rsuang, (1968), Turbulence in the atmospheric boundary layer above steppe and sea surfaces, Atmos. and Oceanic Physics, *4*, 1026-1041.

Wendell, L. L., (1970), A preliminary examination of meso-scale wind fields and transport determined from a net-work of towers, NOAA Tech. Memo., ERLTM-ARL 25, Air Resources Laboratories, Silver Spring, Maryland.

Yanskey, G. R., E. H. Markee, Jr., and A. P. Richter (1966), Climatography of the National Reactor Testing Station, IDO-12048, U. S. Atomic Energy Commission, (Idaho Falls, Idaho).

APPENDIX A

REVIEW OF REACTOR SAFETY ANALYSIS REPORTS

The Air Resources Environmental Laboratory in Silver Spring, Maryland, and the Field Research Office in Idaho Falls, Idaho, have continued to take an active part in the review of reactor safety analysis reports as well as consultations during the preparation of the reports. In addition, written comments have been prepared for the following reports:

Silver Spring, Maryland

1. Enrico Fermi Atomic Power Plant Unit 2, The Detroit Edison Company Preliminary Safety Analysis Report, Amendment No. 3 dated May 11, 1970, and Amendment No. 11 dated October 1, 1970.
2. Atlantic Richfield Company Processing Center Safety Analysis Report, Volumes I and II dated October 29, 1970.
3. Farley Nuclear Plant Units 1 and 2, Alabama Power Company Preliminary Safety Analysis Report, Amendment No. 6 dated October 6, 1970.
4. Fort St. Vrain Nuclear Generating Station, Public Service Company of Colorado Final Safety Analysis Report, Volumes I through IV dated November 4, 1969, and Amendment 17 dated December 21, 1970.
5. Enrico Fermi Atomic Power Plant Unit 2, The Detroit Edison Company Preliminary Safety Analysis Report, Amendment No. 13 dated December 4, 1970, and Amendment No. 15 dated January 27, 1971.
6. San Onofre Nuclear Generating Station Units 2 and 3, Southern California Edison Company Preliminary Safety Analysis Report, Volumes I through IV dated May 28, 1970, and Amendment No. 3 dated November 23, 1970.
7. Three Mile Island Nuclear Station Unit 1, Metropolitan Edison Safety Analysis Report, Amendment 15 dated December 16, 1970, and Amendment 20 dated May 26, 1970.

8. McGuire Nuclear Station Units 1 and 2, Duke Power Company Preliminary Safety Analysis Report, Volumes I, II, and III dated September 18, 1970, and Amendment No. 5 dated May 25, 1971.

Idaho Falls, Idaho

1. Preliminary Safety Analysis Report for the Loss of Fluid Test Reactor.
2. Final Safety Analysis Report for the Power Burst Facility.

APPENDIX B

PUBLICATIONS AND REPORTS

Angell, J. K. (1971), Helical circulations in the planetary boundary layer, J. Atmos. Sci., **28**, 135-138.

Angell, J. K., P. W. Allen, and E. A. Jessup (1971), Mesoscale relative diffusion estimates from tetroon flights, J. Appl. Meteor., **10**, 43-46.

Angell, J. K., D. H. Pack, C. R. Dickson, and W. H. Hoecker (1971), Urban influence on nighttime airflow estimated from tetroon flights, J. of Appl. Meteor., **10**, 194-204.

Angell, J. K., D. H. Pack, W. H. Hoecker, and N. Delver (1971), Lagrangian-Eulerian time scale ratios estimated from constant volume balloon flights past a tall tower, Quart. J. Royal Meteor. Soc., **97**, 87-92.

Bernstein, A. B. (1970), The calculation of turbulent fluxes in unsteady conditions, Quart. J. Royal Meteor. Soc., **92**, 762.

Dickson, C. R., and G. E. Start (1970), Measurements of vortex wake characteristics of large aircraft, U.S. Dept. of Commerce Interim Report, Contract No. DOT-FA70NA-AP-73.

Kao, S. K., C. Y. Tsay and L. L. Wendell (1970), The meridional transport of angular momentum in wavenumber-frequency, J. of Atmos. Sci., , 614-626.

Markee, **E.** H., Jr. (1971), Studies of the transfer of radioiodine gas to and from natural surfaces. NOAA Tech. Memo. ERL ARL-29.

Sagendorf, J. F., S. K. Kao, and C. Y. Tsay (1970), The large-scale meridional transport of sensible heat in wavenumber-frequency space, Tellus **2**.

Sagendorf, J. F., S. K. Kao, and C. Y. Tsay (1970), The kinetic energy of large-scale atmospheric motion in wavenumber-frequency space: II. Mid-troposphere of the southern hemisphere, J. Atmos. Sci., **27**, 1008-1020.

Start, G. E. (1970), Comparative diffusion and deposition of uranine dye, molecular iodine gas, and methyl iodide gas, Proceedings of fifth annual midyear tropical symposium on health physics aspects of nuclear facility siting, Health Physics Society.

Start, G. E., and C. R. Dickson (1970), Wingtip vortex diameters, tangential speeds, and horizontal transport within the first 100 feet above the ground, U.S. Dept of Commerce Final Report, Contract No. DOT-FA70NA-AP-73.

Wendell, L. L. (1970), A preliminary examination of mesoscale wind field and transport determined from a network of wind towers, NOAA Tech. Memo. ERLTM-ARL 25.

APPENDIX C

LABORATORY PERSONNEL

Idaho Falls, Idaho

Mr. Earl H. Markee, Jr., research meteorologist at this station since 1962 transferred to the Division of Reactor Licensing, AEC, at Bethesda, Maryland, in August 1970.

Miss Kae Sidle, mathematician, resigned on October 10, 1970, to work for the Health Services Laboratories, AEC ID.

Mr. Mark Rencher, meteorological aid, resigned on October 21, 1970, from a temporary support position at the Goldburg field site.

Mr. Jerrold F. Sagendorf entered on duty on November 30, 1970, to fill the vacancy left by Mr. Earl Markee.

Mr. Norman Ricks returned to duty February 1 through March 25, and left to register at the University of Utah in Salt Lake City.

Mrs. Loretta Marshall entered on duty on March 25 to extract the time motion analysis data of filmed tetroon flights inside the Idaho State University minidome. She resigned on June 7.

Mr. Sidney Williams, electronics aid, entered on duty April 8 in support of the Goldburg observational program. He resigned on May 28, 1970.

Mr. Kim Marshall entered on duty April 26 for temporary duty at the Goldburg site.

Mr. Delbert Sharp, meteorological technician, transferred with a promotion to the National Weather Service Office at Winslow, Arizona, on May 3, 1971.